Optimized operation of the MTT EnerTwin in non-continuous or part load operation

Magdalena Maj

Thesis to obtain the Master of Science Degree in

Energy Engineering and Management

Supervisors: Prof. José Maria Campos da Silva André

Prof. Krzysztof Pikoń

Examination Committee

Chairperson: Prof. Edgar Caetano Fernandes

Supervisor: Prof. José Maria Campos da Silva André

Member of the Committee: Prof. João Eduardo de Barros Teixeira Borges

November 2017

Contents

Acknowledgments

I wish to express my gratitude to my supervisor Prof. José Maria Campos da Silva André for his valuable input and great support at any time throughout my work. Without Professor's participation, this work would have no value.

I would also like to thank Dr hab. inż. Krzysztof Pikoń – my SUT supervisor for tackling my problems connected with various academic issues.

I would like to thank my supervisor Mark Oostveen at MTT Micro Turbine Technology for giving me the opportunity to carry out this work and to help me with ideas and inspiration along the way. I would also like to thank everyone at MTT for welcoming me and being always open for a discussion.

I would like to express my gratitude to InnoEnergy Master School for the support during the whole study program. I thank the InnoEnergy officials for granting me these magnificent years full of experience, discoveries and challenges, and for opening the doors of opportunities for me.

Finally, yet importantly, my gratitude goes to my family, friends and especially my beloved one for being the most important part of my life while I have been on my way towards this important achievement. I thank God for having such people in my life

Magdalena Maj, Lisbon, October 2017

List of figures

List of tables

List of abbreviations

BV – Buffer vessel

CCHP – Combined cooling, heat, and power

CHP – Combined heat and power

DER – Distributed energy systems

DG – Distributed generation

EU – European Union

ICE – Internal Combustion Engine

LHV – Lover Heating Value

LVM – LabVIEW Measurement

MT – Micro Turbine

MTT – Micro Turbine Technology

NG – Natural Gas

NPV – Net Present Value

PEMFC – Proton Exchange Membrane Fuel Cells

PES – Power Electronics and Safety

PM – Prime Mover

PV – Photovoltaic system

RES – Renewable energy sources

SHW – Sanitary hot water

SOFC – Solid Oxide Fuel Cells

SQL – Structured Query Language

SP – Set point

TES – Thermal energy storage

TET – Turbine Exit Temperature

TOE – Ton of Oil Equivalent

TRNSYS – Transient System Simulation Tool

UK – United Kingdom

US – United States

Abstract

The presented work was performed to study the micro-CHP performance in order to maximize its efficiency while complying with the heat demand. An optimal strategy had to be found between the reduced electrical efficiency and power at part load in comparison with the start/stop and standby losses during intermittent operation.

The work starts with a general study of the MTT's micro-CHP system and obtaining an overview of full load, part load, start/stop and standby powers. Experiments of the system were performed under various conditions, different electrical loads and various initial temperatures of the system. Calculations of the tests results are the electrical energy and thermal energy produced, and fuel consumed. In the work, three operating modes of the system were distinguished: start (heating up), steady state and stop (cooling down). Electrical, thermal and fuel energy were expressed by functions dependent on the load and operational time. Energy functions in different modes of the micro-CHP were used to build the numerical model of the system. Simulations of the model were performed for two different heat demand profiles. The numerical model made it possible to compare the efficiency of the system at full load and at part load and, therefore, to optimize the system's performance in these two operation modes. The conclusion is that it is more efficient to operate the system in full load in terms of economic benefits.

Keywords: micro-CHP, buffer vessel, part load, transient, optimization, numerical model

Resumo

O perfil óptimo de operação é aquele que maximiza a eficiência e satisfaz os requisitos relativos ao calor a fornecer. Obtém-se uma estratégia óptima como um compromisso entre uma menor eficiência eléctrica e uma operação a carga parcial, em vez de maiores perdas no arranque, na paragem e nos tempos de vazio, com funcionamento intermitente.

Apresenta-se um estudo genérico do sistema MTT micro-CHP, quantificando o funcionamento à carga máxima, com carga parcial e as operações de arranque, de paragem e standby. Estes resultados são usados para descrever o comportamento do sistema e obter relações úteis para definir a estratégia de controlo ideal. O desempenho da instalação foi representado com base em ensaios realizados em várias condições, com diferentes cargas eléctricas e temperaturas iniciais. As principais variáveis medidas são a energia eléctrica, a energia térmica produzida e o combustível consumido. As curvas do sistema obtiveram-se por ajuste do conjunto de valores medidos, para determinadas cargas e temperaturas iniciais. O sistema possui três modos de operação: arranque (aquecimento), funcionamento em estado estacionário e arrefecimento. As funções de energia produzida nos diferentes estados do sistema foram usadas para construir o modelo numérico do sistema. Neste modelo, a operação do sistema depende de dois perfis de carga térmica. O modelo numérico permitiu comparar a eficiência do sistema a plena carga e a carga parcial e portanto optimizar o desempenho do sistema nestes dois modos de operação. A conclusão é que, do ponto de vista económico, é mais eficiente operar o sistema em plena carga.

Palavras-chave: micro-CHP, armazenamento de energia térmica, carga parcial, transiente, optimização, modelo numérico

1. Introduction

1.1. Motivation

Distributed energy resources (DER) are expected to play a significant role in the future of the electricity supply. The DER's concept embraces three subconcepts: distributed energy storage, distributed generation of electricity (DG) and load management, i.e. controllable energy loads. DG technology examples are micro-CHP, small wind turbines, photovoltaic systems and other small renewable energy sources, like biogas digesters. Drivers for DG have increased energy efficiency due to co-generation options and fewer line losses, fuel diversification and autonomy, environmental benefits like carbon emissions reduction by the use of RES and more efficient usage of fossil fuels, and reduced investment risk. Additionally, placing a generation close to demand is increasing the reliability of delivered electricity and quality of power. Micro-CHP can play a key role in supporting crucial policy objectives such as market liberalization, increasing shares of the electricity generation from renewable sources, mitigating climate change and magnifying energy savings [1]. Countries like the Netherlands have a high investment potential for micro-CHP where most of the residential space heating and hot water comes from the conversion of natural gas in boilers.

The main barrier to adoption of micro-CHP is the high initial cost. Economic aspects of micro-CHP have been investigated by many researchers. According to [2], the typical micro-CHP system can cost about 500 $/kW and the generation cost can be 45 – 50 $/MWh. The operating costs can be reduced by applying optimized profile of the micro-CHP operation with thermal energy storage. There are several impacts on the economic performance of the plant that is comprehensively discussed in [1]. The paperwork is based on the micro-CHP plant equipped with thermal energy storage and additional boiler. It is worth to point out the various schemes of applications with micro-CHP [3]. Micro-CHP can be coupled with a cooling unit or other heat or electrical power generation unit, such as fuel cells, heat pumps, renewable energy sources [4].

1.2. Objectives

The objective of this Master's Thesis is to study the performance of the micro-CHP system coupled with a thermal storage tank in order to maximize the unit's efficiency while complying with the heat demand. In order to achieve this, tests of the system have to be performed for various loads and initial system temperatures. Analysis of the measurements should lead to obtaining the relations, which will be used as a guideline for the optimal control strategy. The system operation should be compared in part load and in full load.

1.3. Organization of the thesis

The work consists of six chapters. The first chapter 'Introduction' includes an overview of the general issues related to a micro-CHP and the objective of the work as well as the motivation and the present subchapter

– organization of the Thesis. The second chapter includes a literature review of the micro-CHP plant, its potential applications as well as the review of the optimization techniques for improving the micro-CHP performance. In the third chapter, the characteristics of the MTT's micro-CHP unit are discussed. In the same chapter, the experimental results are presented. In the fourth chapter, the numerical model of the system is presented together with the discussion of the heat demand profiles. The fifth chapter presents the results of the simulations of the numerical model. Finally, in the last chapter, the conclusions of the whole work done in the Thesis are presented.

2. Literature review

2.1. Micro turbines

There are different definitions of micro-CHP or micro-cogeneration. According to the European Cogeneration Directive micro-CHP are all units with an electric capacity less than 50 kW [5]. Micro-CHP run usually to produce heat for space heating and hot water in the residential or commercial building and small industries. It can replace conventional boilers. Unlike boilers micro-CHP produce electricity together with heat at high efficiency, using the same fuel, reducing greenhouse gas emissions and lowering electricity prices. Micro-CHP can operate in parallel to the electricity network, meaning consumers can still receive some electricity from the grid but produced electric energy can be exported to the grid. The system can also operate as a stand-alone unit.

The growth of micro-cogeneration was simulated by generous government subsidies. Since the production of power for CHP installations is more efficient than in separate units, it is an instrument for some countries to meet the EU requirements. Cogeneration technology has been developed not only in numbers produced but also in sizes. First plants had a rated power of hundreds of MWe, evolving from hundreds of kilowatts down to 1kWe. The creation of a profitable micro-CHP application is possible in such countries as the Netherlands, where the price of electricity and natural gas on the energy basis is significant. The key target markets are such countries as UK, Germany, the Netherlands, Italy, France, Belgium, Ireland, and Denmark. In the UK, there is the widest range of CHP starting from 1 kWe to the largest units of 740 kWe [6].

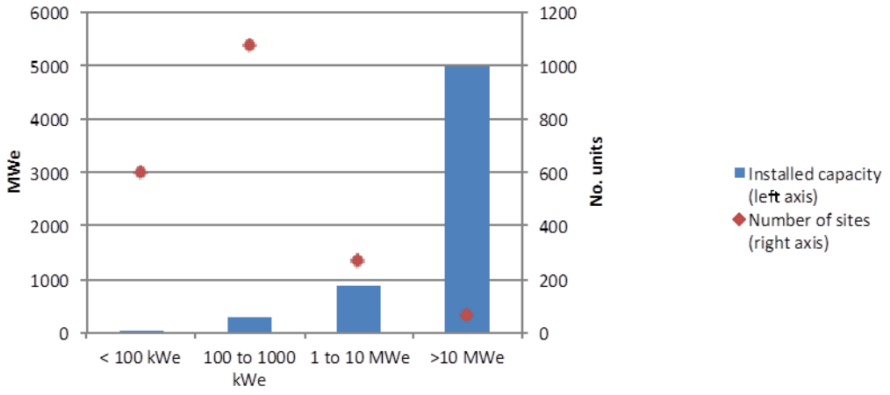

Figure 1 An example of the range of capacities of CHP in the UK (2013) [6]

In the EU CHP is widespread. Units of several hundred megawatts can be found in refining and chemical industry and in a relatively smaller number of large district heating applications. From Figure 1 it can be noticed that the majority of CHP units by number are under 10 MWe, fulfilling heat demand of food and paper industry or serving for smaller heat demand in hospitals, greenhouses and university campuses. Around a kilowatt of electricity from micro-CHP was brought on the UK market in the last decade. Micro-

cogeneration is an option for the small-scale provision of heat and electricity in the residential and commercial sector.

Micro-CHP uses the following types of engine:

- Internal combustion engine (ICE), which already exists on the market
- External combustion engine, usually Stirling, Rankine cycle or steam engines
- Fuel cells, that are still in the development or demonstration stages.

At present, the cogeneration technology on a small-scale base mostly adopted ICE. However, in the last decade, micro turbine is significantly increasing its market shares. The rising success of MT is due to its perfect modularity and useful flexibility characteristics (especially when it is used in clusters). These features make MT suitable for a wide range of loads, applications and fuels. Additionally, in terms of CO and NOx emissions, MT performance in comparison with ICE is better in full load operation [7]. Therefore, micro-CHP with MT can be more often encountered for instance in urban areas, where there are specific environmental restrictions.

Fuel cells are an interesting example of available micro-CHP technologies that might fit well to the future concept of low-energy building, due to their potentially high electric efficiency. An interesting option is also combining fuel cells in a hybrid with turbines. In this context, the leading country is Japan, where the government is strongly supporting this technology by providing grants for new applications. Currently, the technology is still too expensive to be exploited in a broad market. Most of the fuel cells micro-CHP employ proton exchange membrane fuel cells (PEMFCs) that do not operate during the night and are implemented with the battery storage. However, solid oxide fuel cell (SOFC) is expected to be commercialized within a few years. Advantages of SOFC are higher efficiencies (compared to PEMFC) and the possibility of using a variety of fuels [8].

Currently, with the diffusion of DERs, new technologies for cooling power generation are developed around the world and the performance of the existing ones is being improved. This is mostly due to the increasing demand for air conditioning that has stimulated the cooling equipment market. Moreover, cooling is generally needed during electricity peak hours, when the electrical load is higher. With this, electrical cooling loads have contributed to electricity peaks, network overloading and, due to this, failure in electric systems all over the world. Additionally, energy prices (i.e. electricity, oil, natural gas) have significantly increased in many countries due to several reasons, including political interaction with the counties that hold the majority of fossil fuels resources, and inefficient operations on energy markets. This has built up the awareness of governments, communities, and industries about environmental and energy issues and pushed further to search for more efficient applications for local energy generation [3]. Many technologies for cooling and heating available nowadays can be electricity-fired or heat-fired. This allows various combinations with CHP units. The demand for electricity, heat and cooling results of the need of development of trigeneration systems also identified as combined cooling, heat and power (CCHP) plants. Typical trigeneration

application consists of coupling a CHP prime mover (PM) to an absorption chiller fed by cogeneration heat. In such application, extracted heat power is used also in summer to produce cooling. Therefore, the infrequency of adequate thermal demand through the whole year, which is a big disadvantage of cogeneration systems, is fulfilled by transformed cooling demand into thermal demand. As a result, PM can run for a longer time in a year with higher average power, which contributes to optimized control strategies and design, better energy and environmental performance and reduced investment payback time [9]. Obviously, to make trigeneration system economically profitable, adequate thermal demand in winter and cooling demand in summer are needed. With respect to this, potential small applications include hotels, hospitals, schools, food industry, offices, commercial buildings and residential districts etc., and on a larger scale, for example, airports. Different solutions can be applied to the production of local cooling beside absorption chillers with cogeneration heat. Chillers may also be electrically or engine-driven The analysis of different trigeneration systems (schemes and components) may be very interesting when cooling is needed not only for air conditioning or not only for the summer time. In this context, it is worth to notice, that most of the cooling generation equipment is reversible, so it can operate in both mode: heat mode and cooling mode. This improves the plant economy and simplifies the plant schemes [4]. The enthalpy levels at which thermal or cooling power can be produced may be varied when considering combining CHP with different thermal and cooling generation technologies. As an example, cogeneration source such as ICE can produce heat for sanitary hot water and steam to feed absorption chiller, while heat generation source, such as electric heat pump can be used to produce heat for space heating. Therefore, it is possible to distinguish cases of trigeneration and quad generation, i.e. multigeneration, when considering physical carries that transport different forms of energy. Multigeneration can be referred here as production of heat, electric and cooling power, where heat and electric power is at different enthalpy levels (pressure/temperature). What is more, the multigeneration concept can cover the idea of additional output, namely, dehumidification, production of hydrogen or other substances used in specific chemical processes [3]. The overall picture shows a wide range of possibilities to set up local energy systems for a variety of produced energies. Effective planning of combinations of these alternatives can result in benefits in terms of economic profitability, environmental protection, energy efficiency, reliability and quality of the provided service for the end-user.

Traditionally, the term ‘cogeneration’ is associated with power generation from fossil fuels. However, other sources can be adapted to cogeneration, namely solar power, allowing for clean and high-performance solutions. An Interesting concept is combining renewable sources and fossil fuel micro-CHP, even though renewable sources provide intermittent energy generation. The flexibility of combining various scales CHP plant with volatile energy resources as wind power can increase overall efficiency and economic performance of the integrated equipment. Additionally, by adding PV source even higher performance can be reached [10]. Further advantages can be gained through the installation of reversible electrical heat pumps to balance the possible excess of electricity from renewable sources for cooling or heat generation.

In any case, an interesting economic benefit is exposed by the possibility of selling the electricity excess to the grid with the feed-in tariff according to the environmental regulations.

2.2. Micro-CHP system modeling and optimization

An optimization technique is widely used in engineering, science, economy, business, and medicine. In engineering, there are specific fields where optimization is commonly used: searching for the optimal trajectory of space machines, minimization of aircraft weight, designing of turbines, heat exchangers and pumps for its maximum efficiency, optimization in production and planning, optimization in electrical networks and in pipeline networks etc.

Many authors evaluated the economic benefits of micro-CHP system. They pointed out that the feasibility of this technology strongly depends on the user's heat and electricity demand, the fuel prices and the feed-in tariff, as well as on the appropriate sizing of the prime mover and the thermal storage system.

[11] addressed the optimization of the micro-CHP for residential purposes installed in Italy and operating only during winter time. The system there is equipped with a prime mover fed by natural gas, a thermal energy storage, and an auxiliary boiler. Two heat demand-driven strategies of micro-CHP work were implemented in the paper in order to maximize the revenue of the system in comparison to the separate power generation. The first one assumes that the heat is produced from the prime mover to satisfy the user's requirements and to fill up the TES in one-hour step. In the second strategy, there is the possibility of dumping part of the heat produced by PM. To solve the problem two software's were used: Matlab and TRNSYS 17. In Matlab, there was created a code for the economic optimization while the commercial software TRNSYS was used to dynamically model the micro-CHP system. In the work, the hypothesis of PM working only in full load was reported. The operation in part load mode was not considered. The authors take into account incentives that depend on the amount of saved TOE by the micro-cogeneration system and discuss sensitivity analysis on the system with the incentives. Another Italian [12] underlines the benefits of the cogeneration system for the efficiency increase in residential buildings in terms of the EU politics. The aim is to optimize the power plant design in order to minimize the daily power production costs and environmental impacts. In this case, the power plant is equipped with micro-CHP and an absorption chiller, both coupled with thermal storage unit applied to the residential household. The user's profile is considered for different seasons of the year. NPV calculation shows an economic advantage in short and long-term coupling the thermal energy storage with micro-CHP loop and in the cooling loop. However, this gain is not sufficient and it is greater for bigger micro-CHP. Modification of the thermal storage volume did not show a significant impact on the results. In terms of environmental protection, it states that around 7% of the primary energy can be saved in comparison to the district electricity production in Italy and in not more than 3% of CO2. Similar results are found when changing the volume of the TES. The study presents the optimum case for the larger cooling CHP (CCHP) unit with an adequate electric load [13].The CHP plant operates as an island, meaning it is not connected to the grid and its design and operation maximize

efficiency and minimize investment and marginal cost for the residential neighborhood application. For the purpose of the study, the hourly data about heat, electricity, and cooling were collected and scaled up to meet the requirements of the specific neighborhood. A multi-scale problem was solved using a temporal Lagrangean decomposition with a hybrid Lagrange multiplier updating method. Part load performance of the regenerative micro-CHP system of 100 kW fired with dual fuel natural gas – biomass for residential purposes was discussed in [14]. All the simulations of the part load performance of the plant were performed in Gate Cycle software. Apart from the thermo-economic simulation of the power plan with the different fuels ratio, the conclusion from the paper is that the heat demand driven operation is the most efficient. There has been an interesting study of sensitivity analysis in the design and operation of micro-CHP [1]. There are technical and economic uncertainties that may influence implementation of the micro-CHP on the market. Those uncertainties were applied to the impact analysis and evaluation of the framework to a defined case study system. The mathematical model with which the impacts of the system uncertainties were quantified consists of a micro-CHP unit as a prime mover with an auxiliary boiler, electricity storage, and thermal storage. Only the full load of the power plant operation was considered.

3. Micro-CHP study

3.1. EnerTwin development history and its parameters

3.1.1. Micro-CHP characteristics EnerTwin development history and its parameters

MTT's product is the micro-CHP system with off-the-shelf automotive turbochargers such as a centrifugal compressor, a radial turbine, and oil-lubricated bearings. Together with a fuel system, combustor, and control application, this creates a turbojet engine. Mounting generator on a shaft will work as a turboshaft engine to produce electric power instead of a thrust. High turbine outlet temperature gives rise to install a recuperator to recover exhaust heat. Laboratory conditioned tests proved TET (turbine exit temperature) to be as high as 1050 K depending on the setting conditions. With this around average 20 kW of fuel, power is consumed generating 3.2 kW electric power and 15.6 kW heat power when the reference ambient temperature is 15 ^{o}C.

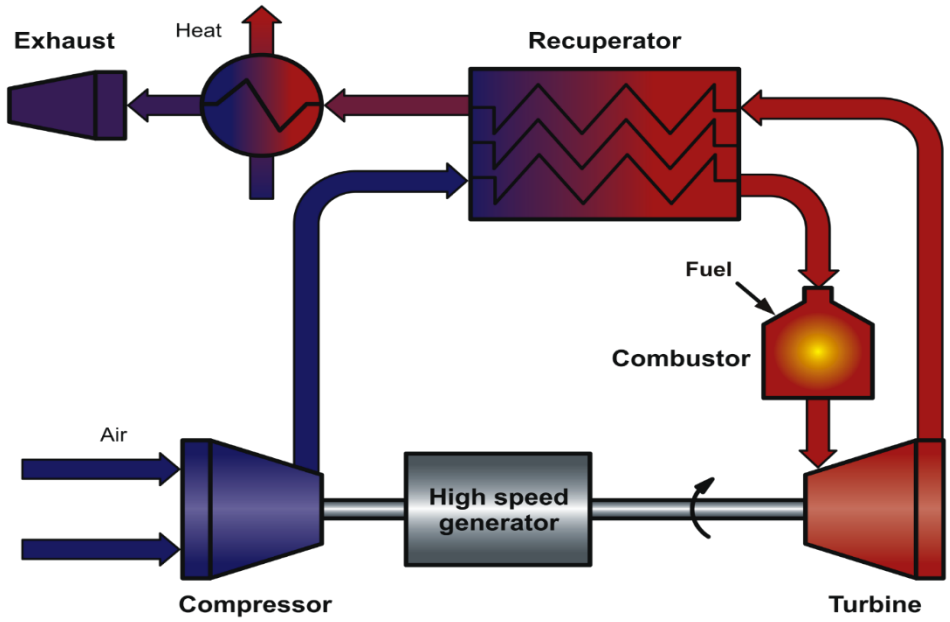

Figure 2 Recuperated micro turbine-based CHP system [15]

Firstly, in 2009 the company could run the unit with a 12.2% electric efficiency, defined as the ratio between the generator's output and the fuel heat input. After excluding electrical losses due to the oil pump, fuel, water pumps, compressors etc., the net electric efficiency was 9.5%. This corresponds to 13.5% shaft efficiency when excluding electrical losses. Next step was to achieve 19.5% generator power efficiency, which refers to 16.5% net electric efficiency and 22% shaft thermal efficiency. This could be done by optimizing components [15].

Table 1 System parameters

		Max.	Min.	
Performance at ISA[1]	Net electric power[2]	3.2	1.0	kW
	Net thermal power	15.6[3]	6.0	kW
	Power to heat ratio at max power	20		%
	Net grid output efficiency	16	10	%
	Total efficiency	> 94.3		%
	Rotor speed	240,000	180,000	rpm
	Fuel flow (H gas, 38.5 MJ/nm^3)	1.87	0.84	nm^3/h
Fuel	Natural gas H, E and L			
Operating conditions	Ambient air pressure	0.8 – 1.1		bar
	Inlet air temperature	–20 – 40		^{0}C
	System room temperature	5 – 40		^{0}C
Heating system	Water flow rate	3 – 21		l/min
	Water return temperature	5 – 60		^{0}C
	Water out/buffer vessel temperature	5 – 80		^{0}C
	Water pressure	0.7 – 4.0		bar
Maintenance	Service interval	1 / 5000		year/ hours
Emissions	NO_x	< 27		ppm @ 15% O_2
	CO	< 50		ppm @ 15% O_2
	CO_2 savings	3 – 6 [4]		tons/year
	Noise	55		dB(A) 1m
Control	OpenTherm heating control interface			
	RS-485 modbus remote control interface			
	0-10V building management system interface			
	MTT proprietary cascade operation control interface			
Installation	Dimensions h x w x d	995 x 600 x 1170		mm
	Weight (empty/with water & oil)	205 / 215		kg
	Inlet air and flue gas pipes	DN 100 (parallel or coaxial)		
	Grid connection	230 / 50		VAC / Hz

[1] ISA conditions at sea level are 15°C and 1.01325 bar.
[2] Net electric power is the power delivered to the grid corrected for internal fan and heating system water pump power, which is separately accounted for according to micro CHP performance rating standards.
[3] Depending on heating system operating conditions, such as water return temperature.
[4] Depending on operating profile.

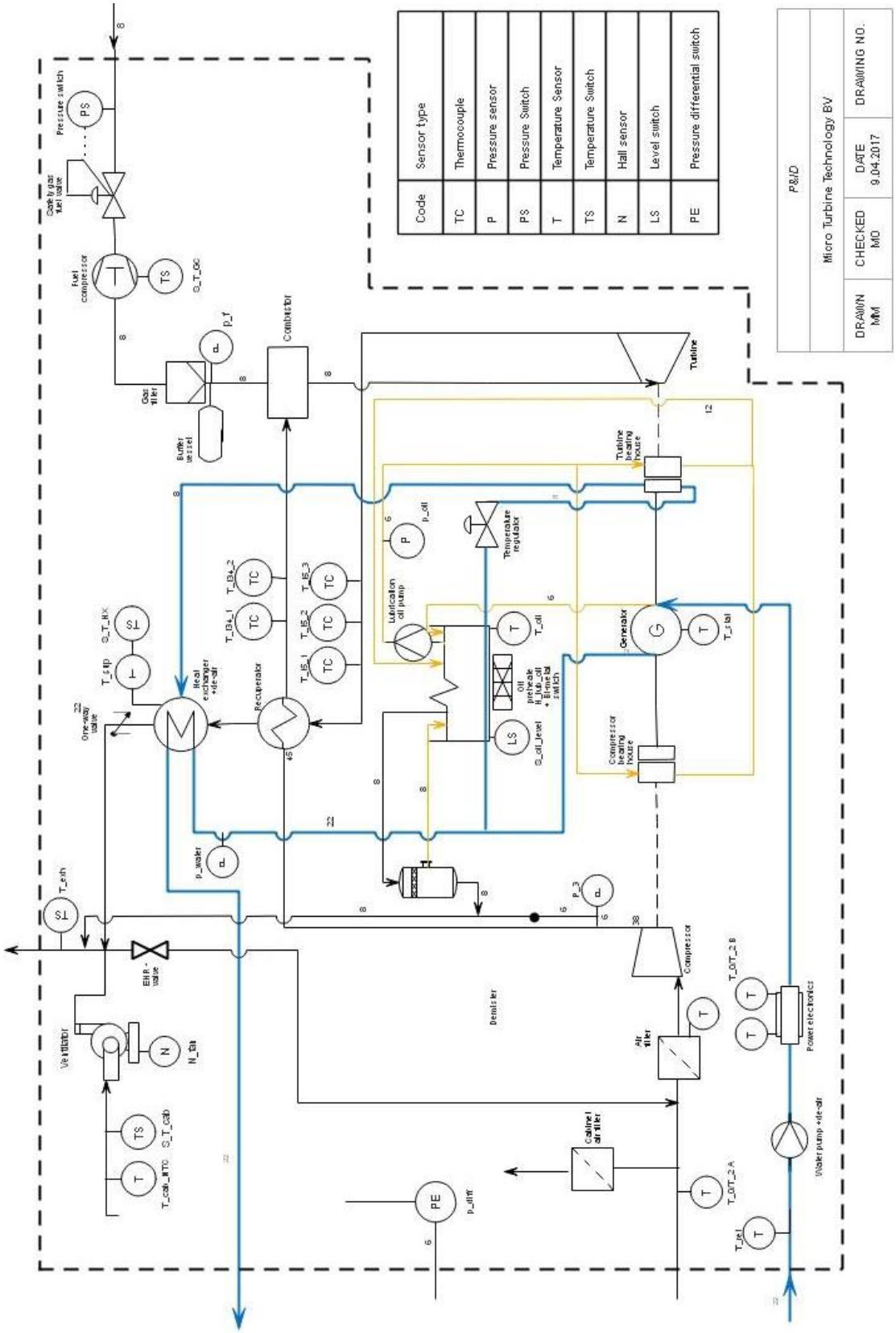

Figure 3 Process and instrumentation diagram

3.1.2. Process and instrumentation diagram with the description

Figure 3 represents the process and instrumentation diagram that we made with a detailed diagram of pipes, instruments and control devices of the industrial process.

On the P&ID diagram, the blue line represents the pathway of water, the yellow color is used for oil, and the black line corresponds to air/gas.

The outside air entering the system is partially supplied to the cabinet through an air filter, while the main stream of air goes to the compressor after filtration. Before combustion, the compressed air is preheated in the recuperator with heat from the exhaust gases. Hot combustion gases are expanded in the turbine, which provides the torque necessary to run the generator and the compressor. After the recuperator, exhaust gases transfer the heat to the water in the heat exchanger. Before being exhausted, part of them may come back to the compressor's inlet.

Water entering the system is pumped and used to cool down the electronic system before flowing to the generator. Next, the water line is split into two streams: one flows directly to the heat exchanger and the other one controls the temperature of the oil sump and, after this, cools down the turbine bearings and finally is further heated in the heat exchanger. The largest amount of heating comes from the exhaust gases.

The pressure switch controls the natural gas valve that supplies power to the valve only if the gas pressure is above a minimum threshold. After this, the fuel is compressed, filtered and transported to the combustion chamber.

The oil pump provides oil to the turbine and compressor bearings. The oil system is equipped with the demister that is sucking out the air from the sump, filtering it and draining oil residues back to the sump and air to the exhaust. The original idea was to use this air for compression, however, it appeared that it was not clean enough and could cause compressor fouling.

The shaft power of a gas turbine is controlled by the air mass flow rate through the turbine and the temperature decrease across the turbine, which depends on the pressure ratio of the turbine. The mass flow rate and pressure ratio vary with the rotational speed of the compressor. The gas temperature before the turbine is (mainly) determined by the fuel flow rate. For a given flow rate of air, there is a limit to the amount of fuel that can be supplied and therefore a limit to the net power output. The working temperature of the highly stressed turbine blades restricts the maximum allowed fuel/air ratio. The EnerTwin fuel flow is controlled by the temperature of the recuperator. Varying the rotational speed and fuel flow, any power between 0 and 3 kW can be obtained. For efficiency reasons, the lower limit is 0.9 kW; the upper power is limited by temperature, maximum turbine speed, maximum fuel flow and maximum electric current.
The desired turbine exit temperature and air mass flow rate delivered by the compressor define the fuel/air ratio. The fuel flow rate supplied to the combustion chamber depends on:

- The temperature of the air before the combustion chamber (which is higher when the system is already operating);
- The difference between the desired temperature and the actual temperature after the turbine and the air mass flow rate (which varies with the rotational speed of the gas turbine).

3.1.3. Thermal energy storage installation

The system can use a heat storage tank (different terms are used interchangeably like accumulator, tank, heat storage, thermal storage, cylinder, buffer vessel). This device stores the water that allows an increase in the total volume available for heating distribution. Thermal storage absorbs the additional heat produced by the system not needed at that moment by the end user. The storage can also separate water circuits. This allows for an optimal control of heat demand. The minimum power output may not be enough to accommodate the demand if the system relies only on the water being presently heated. Thermal energy storage (TES) helps to match the system instantaneous production and the required thermal output. Figure 4 shows the connection of the system with the buffer vessel for direct heating purposes and for sanitary water. The sanitary hot water is heated up in a (plate) heat exchanger in the circuit equipped with a separate water pump. The system can also be connected directly to the floor heating system or to a cascade with more micro-CHP or boilers [16].

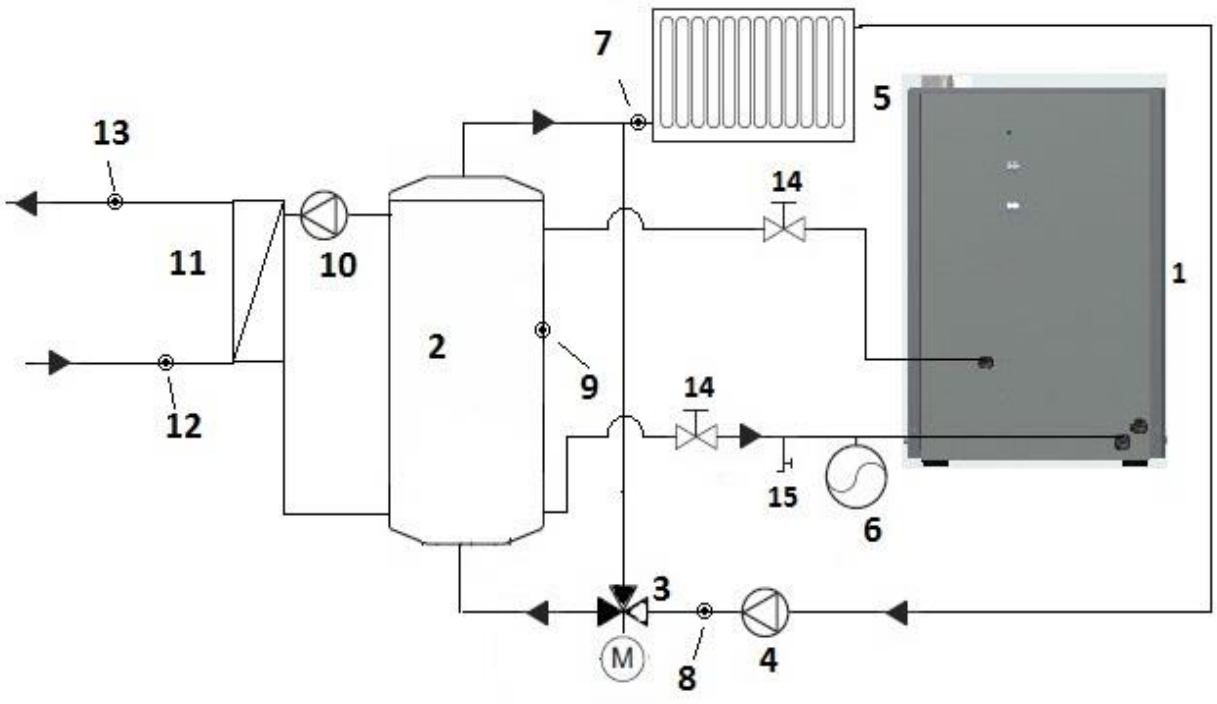

Figure 4 Schematics of EnerTwin for central heating with buffer vessel and radiator [17]

1. Micro CHP
2. Buffer vessel
3. 3-way valve
4. Pump
5. Radiators
6. Expansion vessel
7. CH-supply water temperature sensor
8. CH-return water temperature sensor
9. Buffer vessel temperature sensor
10. SHW Pump
11. Heat exchanger
12. SHW flow meter
13. SHW temperature sensor
14. Valves
15. Fill and drain valve

3.1.4. Heating control with buffer vessel

The operation of the EnerTwin is achieved two controlling systems: gas turbine and heating control. The latter one converts heat demand into the power setting, named setting point (*SP*). *SP* is a parameter in percentage representing a demanded load of the turbine. Gas turbine controls guides the controlled operation and responds to the power settings as demanded by heating control. It is also sending the control settings for subcomponents to the Power Electronics and Safety (PES). PES also monitors the safety threshold and the grid status. In fact, the system is heat demand driven which means it will work only if there is required the production of thermal energy. With the variation of the rotational speed of the turbine, power is controlled and fuel flow is adjusted in order to maintain desired turbine exit temperature.

Table *2* indicates modulation range, thermal and electric power dependencies and control points of parameters. Relations in between given points is linear in two sections; from *SP* = 20% to *SP* = 60% increase in power is higher than for the range of *SP* = 60% up to *SP* = 100%. In the graphical representation of the function *SP* = f(*P_el*) or *SP* = g(*P_th*) the slope of the line for the first section of the curve is smaller than the one for the second section.

Table 2 Modulation range and control parameters

Power setting - *SP* [%]	**Thermal power [kW]**	**Electric power [kW]**	**Rotational speed [rpm]**	**Turbine exit temperature [K] /[°C]**

0	0	0	0	N/A
20	7.6	0.9	180000	1060/787
60	10	1.6	200000	1050/777
100	15.6	3.2	240000	1040/767

When the system is used in combination with a buffer vessel, the modulation of the heat supply from a buffer vessel is obtained by settings the position of the 3-way valve (3) and the speed of the water pump. Heating control rules the charging state of the buffer vessel, 3-way valve, and the water pumps.

There can be several ways of controlling the buffer vessel temperature. The conventional approach that is currently applied by MTT, assumes that only an installed temperature sensor monitors the buffer vessel temperature Tbuf and the turbine operates with its maximum power to charge the buffer vessel. Whenever the desired state of the buffer vessel is reached, the system stops. The control is maintained with a few temperature indicators:

- *Tbuf_max* – the maximum allowed the temperature of the buffer vessel. Thereby also, the maximum water temperature can be supplied from the system to the buffer vessel.
- *Tset* – set point temperature of the buffer vessel. When it is reached, the system should not provide more heat to the buffer vessel.
- *Thys* – buffer vessel hysteresis. It is the temperature difference from *Tset*, below which the system should start operating and heating up the buffer vessel. This drop, equal to *Tset* – *Thys*, is a trigger point to start the system.

The purpose of this thesis is to define the optimal operating schedule and the achievable optimal operating profile. Results should prove if it is profitable to operate the system at part load. An optimal strategy has to be found between reduced electrical efficiency and power at part load in comparison to the start/stop and standby losses during intermittent operation.

3.2. Experimental part

In this section, we aim at finding a function capable of describing the system's performance, in order to optimize its operation under variable loads and evaluate its achievable output. This mathematical model consists of a set of equations that reflect the system behavior. To obtain this functional description, we tested the power plant in transient and steady states, with various loads. After many trials, the system's parameters were found for a wide range of working conditions. Measurements included the heat and electricity production and fuel consumption. Finally, the model was used to find the optimal production strategy, subject to the heat demand restriction.

3.2.1. Experiment methodology

We decided to test the system in a few set points: 20%, 40%, 60%, 80%, and 100% electrical load. An important parameter influencing the start behavior of the EnerTwin is the temperature of the system. MTT uses the temperature of the recuperator (labeled *Tt_34*, measured by a redundant sensor) as the reference temperature of the system. The recuperator reflects the heating state of the system due to its high heat capacity. Depending on this temperature, the starting condition of the system can be considered as cold, warm or hot. Cold start occurs when the temperature of the system is similar to the ambient temperature: the system's components have to be warmed up before delivering heat to the circulating water. This takes time and while the system heats up there is no hot water production. In a warm start, the system is already able to deliver some amount of heat to the water. During a hot start, the system is hot enough to deliver the maximum possible heat to the water almost instantly after starting. To account for the influence of the system temperature, several starts of the system, at various starting temperatures (*Tt_34_0*) were performed: 300 K, 450 K, 600 K, 750 K and 860 K.

3.2.1.1. Electric and fuel energy calculations

3.2.1.1.1. Fuel energy

The raw data measured was logged in the two database systems: SQL and LVM. The latter recorded the measurements from the fuel gas flow meter (Bronckhorst); the fuel flow was recorded every second. That device is not as accurate as the other meter – volumetric gas meter, installed outside of the test's cell. It measured the accumulated gas volume flow rate in cubic meters with a high precision. It was more convenient to use the Bronckhorst flow meter to calculate the instantaneous fuel energy input and verify the result with the more reliable integral measurement. Data was collected constantly while the system was running. For the volumetric gas meter, the measurements were taken at the beginning and at the end of the time period. Four tests were carried out: cold start (*Tt_34_0* = 300 K) and hot start (*Tt_34_0* = 860 K), both for ~1100 s and ~3900 s from the moment of start. Fuel consumption was measured and calculated with two sensors for all tests. The results are presented in the tables below. Table 3 exhibits the values of the fuel energy input. Table 4 and Table 5 show the calculated efficiencies and their relative errors.

3.2.1.1.2. Electric energy

Electric energy was measured in two ways. On one hand, we displayed the accumulated energy production up to the time being, leveraging a digital power meter (Yokogawa). The data from this display was not recorded continuously but only at the beginning and at the end of the period, similarly as with the volume gas meter. On the other hand, we measured and recorded power at a rate of a sample per second, throughout the whole period. We then compared the first method's results with the integral over the results gathered by the second method. These later set of measurements were definitely more convenient to use. The electric and fuel energy measured with different devices are presented in the tables below.

Table 3 Electric and fuel energy calculations over ~3900 s from the moment of cold and hot start

Tt_34_0 [K]	Electric energy [MJ]		Fuel energy [MJ]	
	Integer	Yokogawa	Bronckhorst	Volumetric
~300	10.76	10.79	78.61	79.09
~860	11.75	11.84	77.62	78.08

Table 4 Efficiencies and efficiency relative errors of fuel energy measured by two devices

	Bronckhorst	Volumetric	Efficiency relative error
~3900 s cold start (*Tt_34_0* = ~300 K)	71.94%	71.51%	0.61%
~3900 s hot start (*Tt_34_0* = ~860 K)	82.85%	82.36%	0.59%
~1100 s hot start (*Tt_34_0* = ~860 K)	81.51%	80.10%	1.76%

Table 5 Efficiencies and efficiency relative errors of electric energy measured by two different devices

	Integer	Yokogawa	Efficiency relative error
~3900 s cold start (*Tt_34_0* = ~300 K)	71.94%	71.99%	0.07%
~3900 s hot start (*Tt_34_0* = ~860 K)	82.85%	82.96%	0.14%
~1100 s hot start (*Tt_34_0* = ~860 K)	81.51%	80.98%	0.66%

At the beginning of a cold start, there are important fluctuations of the gas flow rate and energy produced and this reflects a bigger difference between the two measuring systems. During steady-state operation, that difference is practically unnoticeable. Therefore, the longer time-measurements, with a large part of the operation taking place in steady-state conditions, exhibit a smaller overall error. In all cases, the efficiency relative error was smaller than 2%. The largest error (1.76%) related to the fuel energy measurement for the 1100 s hot start. As long as the operational time of the system is not much shorter than 1100 s, there were no concerns about significant errors of electricity or fuel energy.

3.2.2. Test performance

This subchapter presents the results of cold, warm and hot restarts. The tests reported here were performed after some trial tests.

3.2.2.1. Full load

3.2.2.1.1. Overview of the operation at full load

Figure 5 presents the relations between the rotational speed of the engine and the produced electric and thermal power and the consumed fuel power for the cold start at full load.

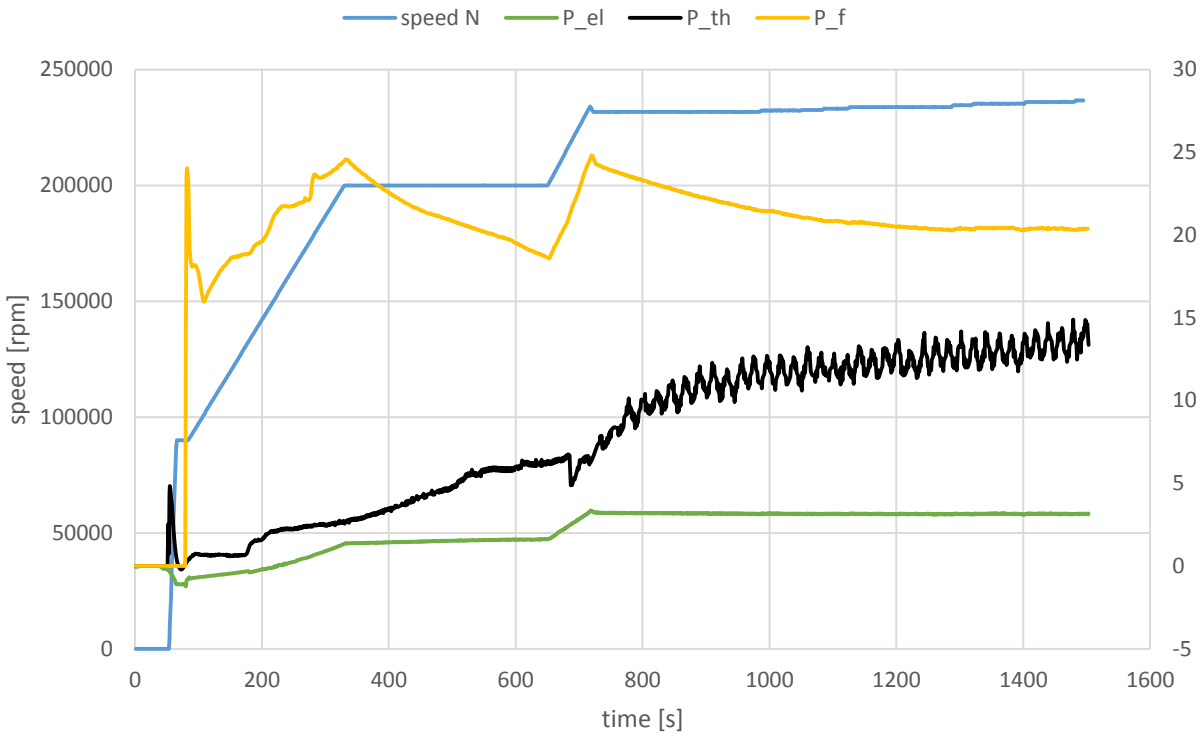

Figure 5 Rotational speed, electric, thermal and fuel power over time for the cold start with full load

The engine sped up until the so-called ignition speed was reached. This moment is visible on the plot of Figure 5, after more than a minute after the start. The ignition speed N_{set} in rpm was set to:

(1)

$$N_{set} = 89000 * \sqrt{\frac{T_0}{288.15}}$$

Where T_0 is the ambient temperature [K]

In Figure 5, there are three peaks of fuel power, with similar values of power, for the cold start (orange line). The first peak occurs during ignition. After ignition, the system accelerates to a speed of around 200 000

rpm and fuel power increases up to the second peak. Then, the engine speed is maintained and the fuel power decreases. The system stays in this condition to heat up the recuperator up to the desired temperature. The more the recuperator is heated, the less fuel must be supplied to warm up the air in the combustion chamber. That is why the fuel flow rate drops while the temperature of the recuperator rises. Then the system accelerates again. The system is controlled to warm up the recuperator at a lower speed and, due to this, consumes less fuel, instead of increasing further the speed. After this step, the system accelerates up to ~240 000 rpm and the fuel consumption rises to reach the third peak. The engine speed is kept constant, depending on the external conditions. The fuel power consumption is minimal when the temperature of the system components is higher: the fuel power stabilizes at around 20 kW.

Electric power follows a similar pattern as the engine speed changes. The electric production is around 1.5 kW when the system reaches the constant speed of ~200 000 rpm.

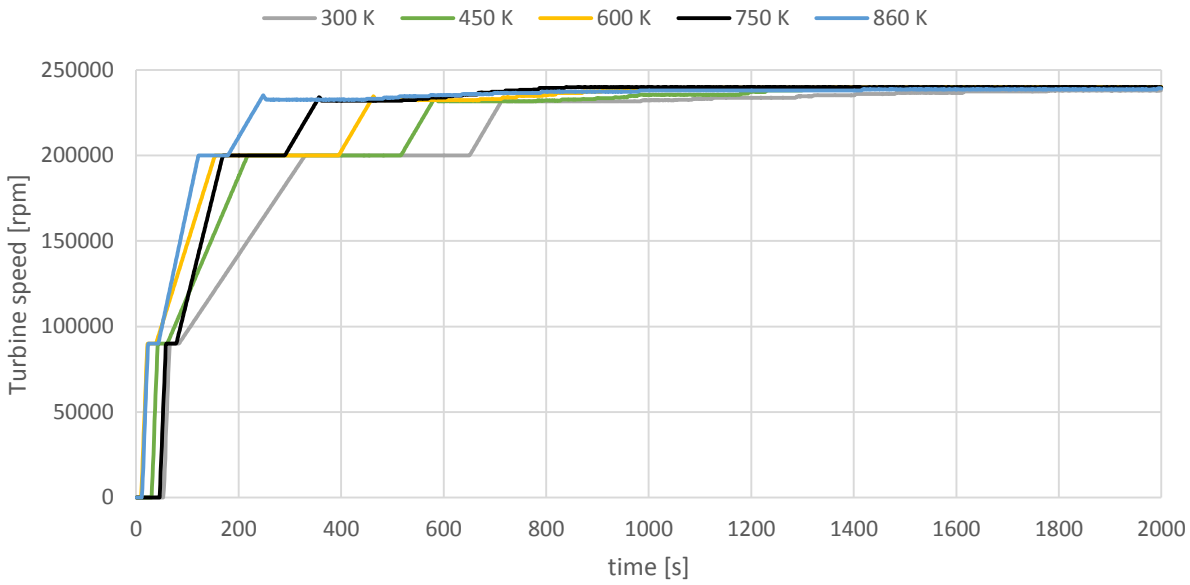

Figure 6 Turbine speed over time for different starting temperatures Tt_34_0

The plots in Figure 6 represent the acceleration of the turbine when the system starts with different recuperator temperatures *Tt_34_0*. The curves differ in steepness and length of the sections, but their pattern is the same. It can be noticed that, for the cold start (300 K), the stage at 200 000 rpm takes a longer time, required to warm up the recuperator. As expected, the time to reach steady state is smaller for a hot start (860 K).

3.2.2.1.2. Electric power

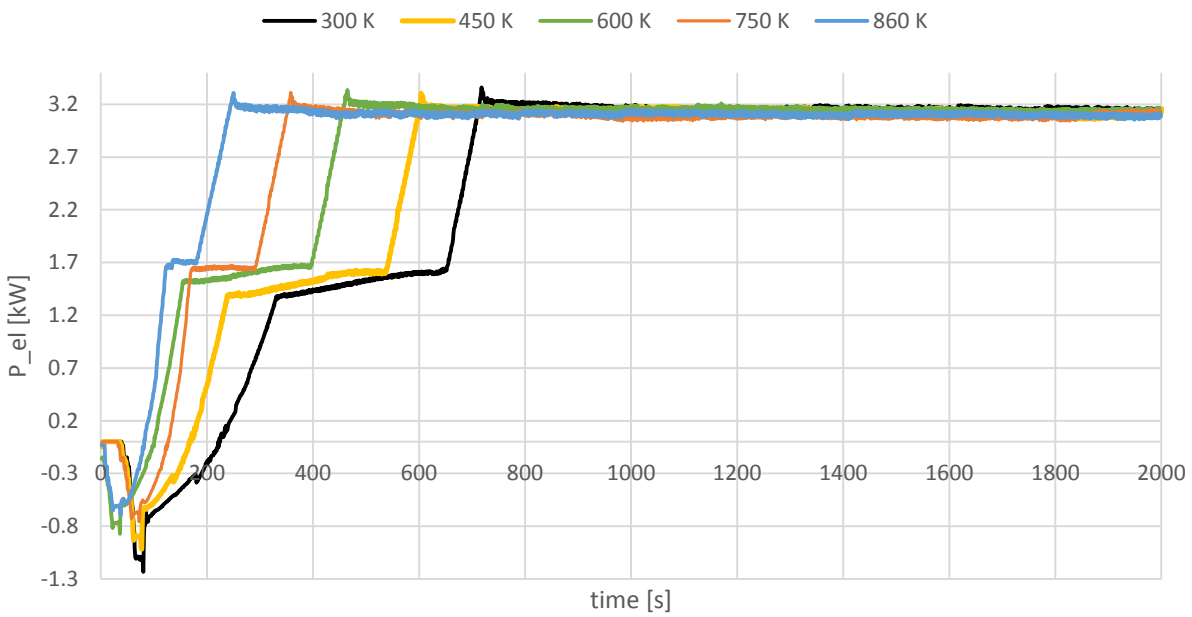

Figure 7 Electric power for starts at full load – set point equal to 100%

Figure 7 represents the electric power production for five starts at different initial recuperator temperatures. During an initial period of time that lasts between 1 and 4 minutes, the plant consumes electric power to drive the turbine; power production begins only after ignition takes place. The profile of this initial electric consumption is similar for all tests. The starting stage is always required because a gas turbine cannot produce torque at zero speed, but the duration varies with the recuperator initial temperature. The highest peak in consumption of electric power during warm-up is for the lowest *Tt_34_0* (cold start), and it is around –1.235 kW (this power is negative), while for the highest *Tt_34_0* (hot start) it is around –0.697 kW. The shortest time to reach the nominal electric power is for the highest *Tt_34_0*, being slightly more than 4 minutes. However, this does not mean that the steady state of the system is already reached at this time.

3.2.2.1.3. Thermal power

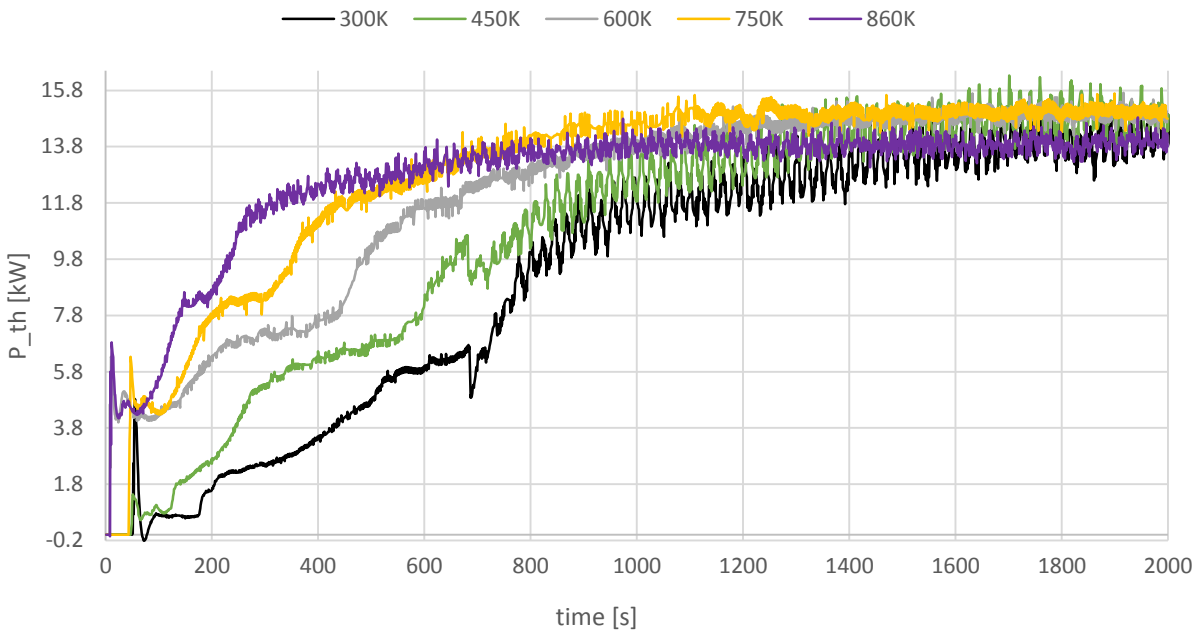

Figure 8 Thermal power for starts at full load – set point equal to 100%

Figure 8 displays the heat power production for the five starts of the system. Heat is calculated from the equation:

(2) $$P\_th = \dot{m}_w * c_p * \Delta T$$

Where:
$\dot{m}_w$ – is the water mass flow rate [kg/s]

c_p – is the specific heat capacity of water [$\mathrm{J/kgK}$]

ΔT – is the temperature difference between water outlet and inlet of the system

The specific heat capacity was taken as constant and equal to 4179 J/kgK, which is the specific heat capacity of the water at 40 ºC. This is the average between the water temperature coming in and the requested water temperature going out of the system. At steady state, ΔT should be equal to 20 ºC. The system can be configured to operate with the water inlet/outer temperature set to: 30 ºC /50 ºC, 40 ºC / 60 ºC or 60 ºC /80 ºC. In all the experiments, the settings were those of the MTT standard water temperatures: 30 ºC /50 ºC.

As expected, during a hot start, the system produces heat almost instantly and reaches the highest rates of heat quicker. There occurs a peak in thermal power production in all the tests (between 0 s and 60 s) because there remains some temperature difference between the temperature sensors of water supply and return. Even for cold start tests, the temperature of the water coming into the power plant is slightly heated up, because the temperature decay of the system takes several days. When the pump starts working, this

pre-heated water comes out of the plant registering a peak of thermal power. Circulating water takes the remaining heat of the system and in a few seconds, the peak disappears. A few seconds after the pump started, the water mass flow rate is soon higher than 0.22 kg/s, exhibiting small oscillations, and the pump rotates at maximum speed. The temperature difference between water coming in and going out of the system increases during all that time, which results in an increase of the thermal power.

3.2.2.1.4. Fuel power

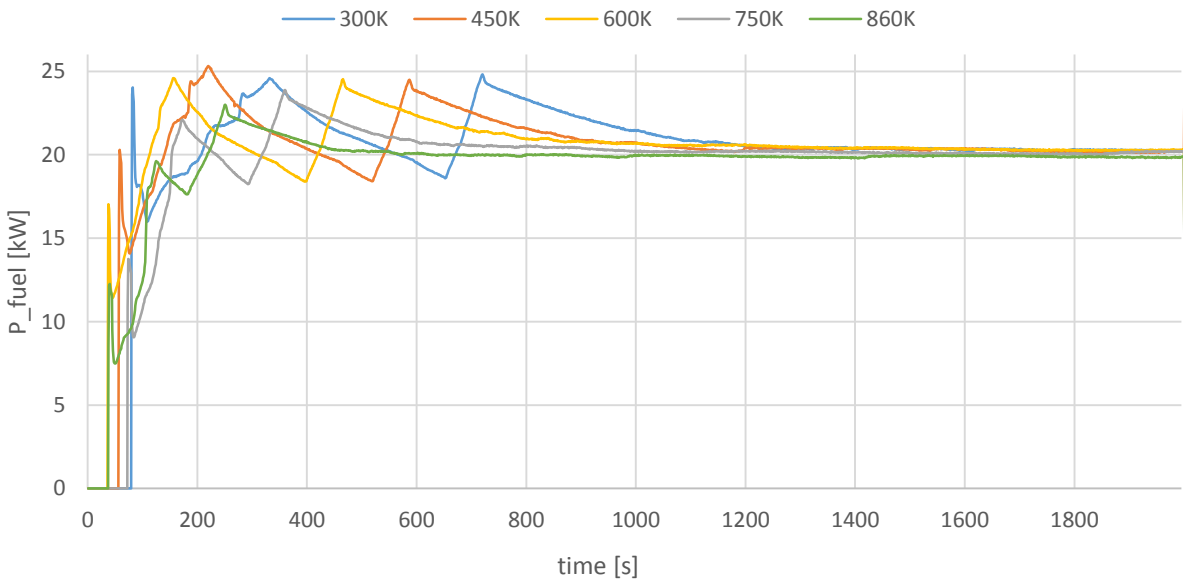

Figure 9 Fuel power for starts at full load – set point equal to 100%

Figure 9 represents the fuel power consumption for the five different starts of the system. The fuel power output is calculated from the equation:

(3) $$P\_fuel = \dot{m}_f * LHV$$

Where:

$\dot{m}_f$ – is the fuel flow rate in kg/s

LHV – is the lower heating value of the fuel [MJ/kg]

The fuel given to the system is a gas containing 81.3% of methane with a calorific value of 30.02 MJ/m^3 and density ρ = 0.79 kg/m^3 at the conditions of 288.15 K and 101.325 kPa. With these conditions, the value of LHV in MJ/kg is equal to 38 MJ/kg.

In the tests, one can distinguish three peaks in the fuel consumption before the steady state is reached. For the cold start, these peaks are slightly below 25 kW, with a maximum of around 24.82 kW. For the hot start, peaks in the fuel power are lower because the system is warmer at the start and there is no need to

supply as much fuel as for the cold start. For the hot start, the maximum peak (~23 kW) occurs after the turbine speed reaches ~200 krpm and the recuperator is heated up.

3.2.2.2. Part load

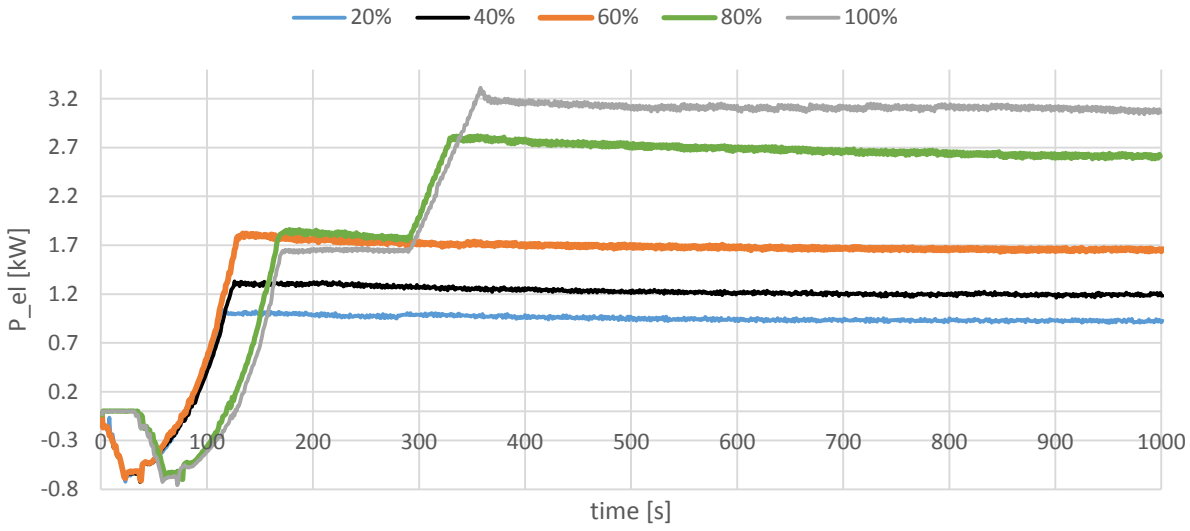

Figure 10 Electric power for start with Tt_34_0 of around 750 K and SP = {20%, 40%, 60%, 80%, 100%}

Figure 10 presents the results of start tests with *Tt_34_0* equal to about 750 K and different loads with corresponding set points = {20%, 40%, 60%, 80%, 100%}. The smaller the electric load, the faster nominal power and steady state are reached. However, for the tests with the *SP* < 60%, the time to reach nominal electricity is almost the same, the difference is about a few seconds. For the possibly lowest and highest electric load with *SP*=20% and *SP*=100% respectively, the time difference to reach nominal power is around 250 s, which is ~4 min.

Part load operation causes efficiency losses. Figure 11 presents the relations in steady state between the electric output and the electric efficiency on the first axis and overall efficiency on the second axis. The electric efficiency (also net efficiency) is calculated as the ratio between the electric power output and the fuel power input, while the overall efficiency is the ratio between the sum of the electric power output and heat power output and the fuel power input. The bigger dots on the plots in Figure 11 represent nominal power at specific set points. Values in between them were estimated by a second-degree polynomial.

Reduction of the full electric load by approximately 50% corresponds to the set point *SP* = 60% and results in an electrical efficiency drop of around 19.4% (a decline from 16% to 12.9%).

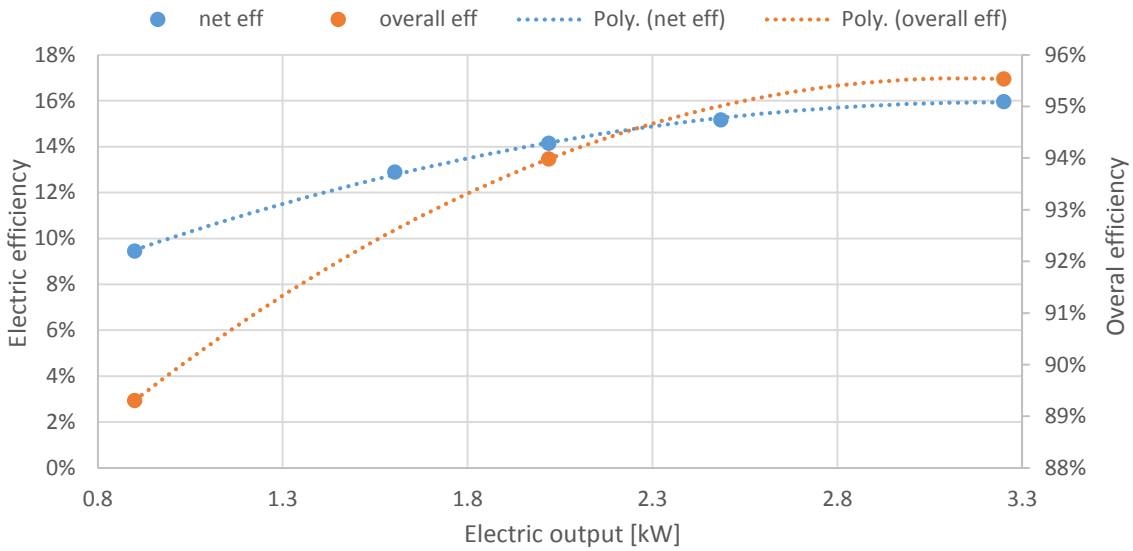

Figure 11 Part load efficiency

3.2.3. Steady state definition

Since the system tends smoothly to steady state operation, we have to define the boundary between the transient and the steady state domain. We assumed that it should be possible to identify steady state conditions by observation of one or more parameters. The recommendation was to choose the recuperator temperature as the reference parameter. The reason is that the recuperator temperature is not affected by small perturbations, because of its high heat capacity. However, the analysis of trial tests proved that it may not be the most effective way to define steady state operation since the recuperator temperature depends on the electric load and the outside conditions. For a full load, it is around ~979 K.

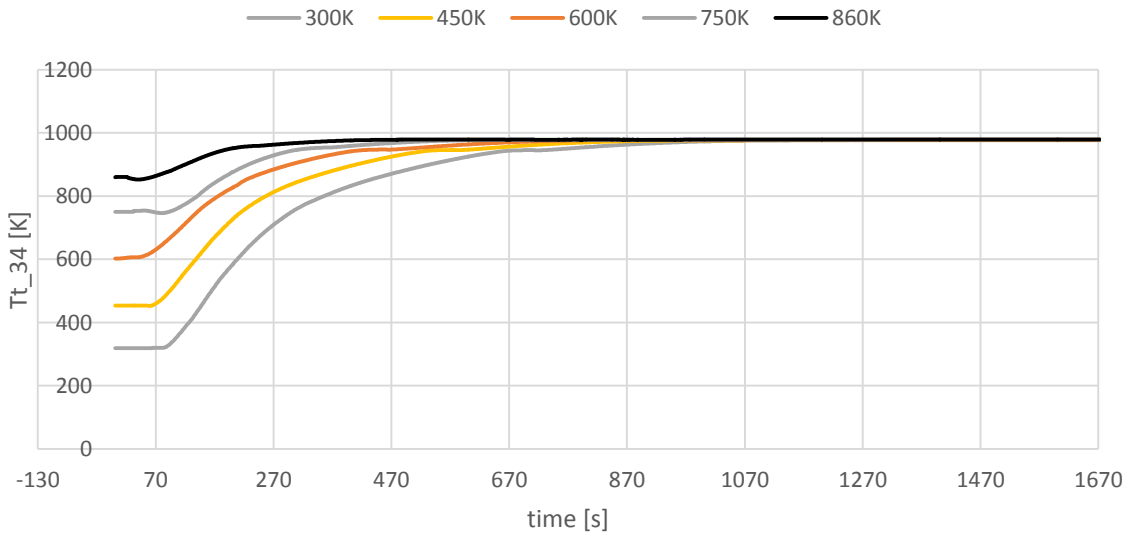

Figure 12 Function of Tt_34 over a time for different starting Tt_34_0 and SP =100%

Figure 12 shows plots of the function *Tt_34*(*t*) for different starting recuperator temperatures *Tt_34_*0. We will see that these curves follow an exponential evolution. Only at the beginning of each test, during a short period of time, part of the plot does not match that exponential fit. In practice, this part is the time interval until the moment when combustion starts. After that, heat is produced and transferred to the recuperator, continuously increasing its temperature. For the cold start with *Tt_34_0* = ~300 K, combustion starts around at 65 s and for the hot start with *Tt_34_0* = ~860 K it starts at around 23 s.

3.2.3.1. Exponential Regression using a Linear Model

This subsection describes the regression used to fit an exponential curve into the function of the recuperator temperature. The difference in temperature ΔT between steady state $Tt\_34_{\_\infty}$ and instantaneous temperature $T(t)$, will be described as an exponential function of the form:

(4) $$\Delta T = Tt\_34_{\_\infty} - T(t) = \Delta T_0 * e^{-\alpha * t}$$

Where:

ΔT_0 – is the initial temperature difference

$Tt\_34_{\_\infty}$ - is the assumed final temperature at steady state

t – is the time since the virtual origin of the exponential decay

α – is a constant

The recuperator temperature stabilizes at around $Tt\_34_{\_\infty}$= 979 K at full load.

After taking natural logarithm on both sides of Equation (5):

(5) $$ln(\Delta T) = -\alpha * t + ln(\Delta T_0)$$

In logarithmic scales, the exponential function becomes linear. Figure 13 represents the recuperator temperature in time and the logarithm of the temperature difference.

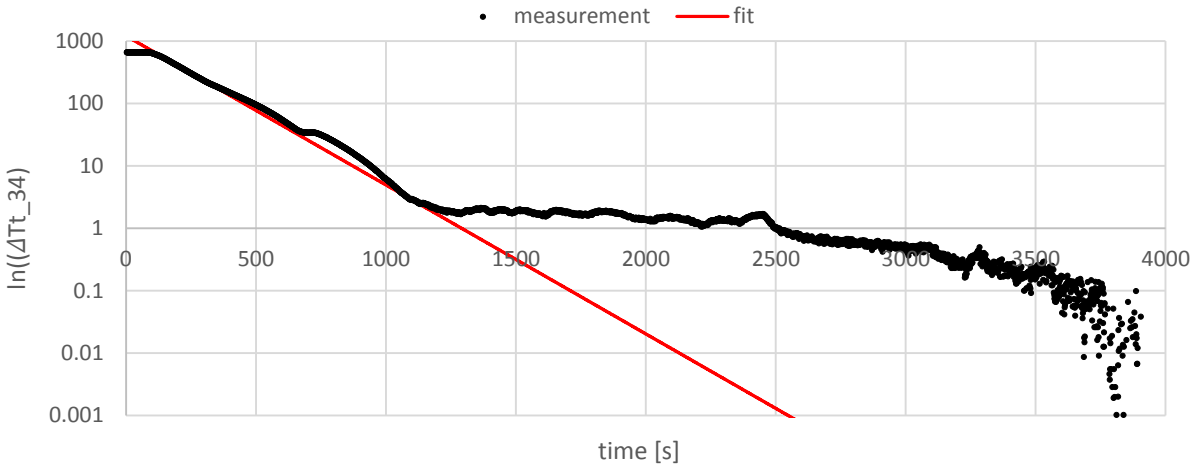

Figure 13 An example of curve fit to ln(TΔ(t))

When the temperature $T(t)$ approaches the steady state $Tt\_34_{\_\infty}$, the relative error of the measurement of the temperature difference tends to infinity and exponential fit looses significance. At some moments, the difference is smaller than the last digit measured and rounds up to zero: these points would appear in Figure 13 as ln(ΔT) = - ∞. In other moments, because of errors, the difference will be negative: those points are not represented in Figure 13. In addition to these difficulties in measuring very small quantities, the automatic control of the system enters into action, sometimes cutting off heating and in other occasions resuming heating: during this stage, the water temperature fluctuates around steady state, sometimes above, sometimes below T_{∞}. When this happens, the rate of increase of the recuperator's temperature follows no longer an exponential fit.

The result of curve fit is plotted on the chart with the regular scale below:

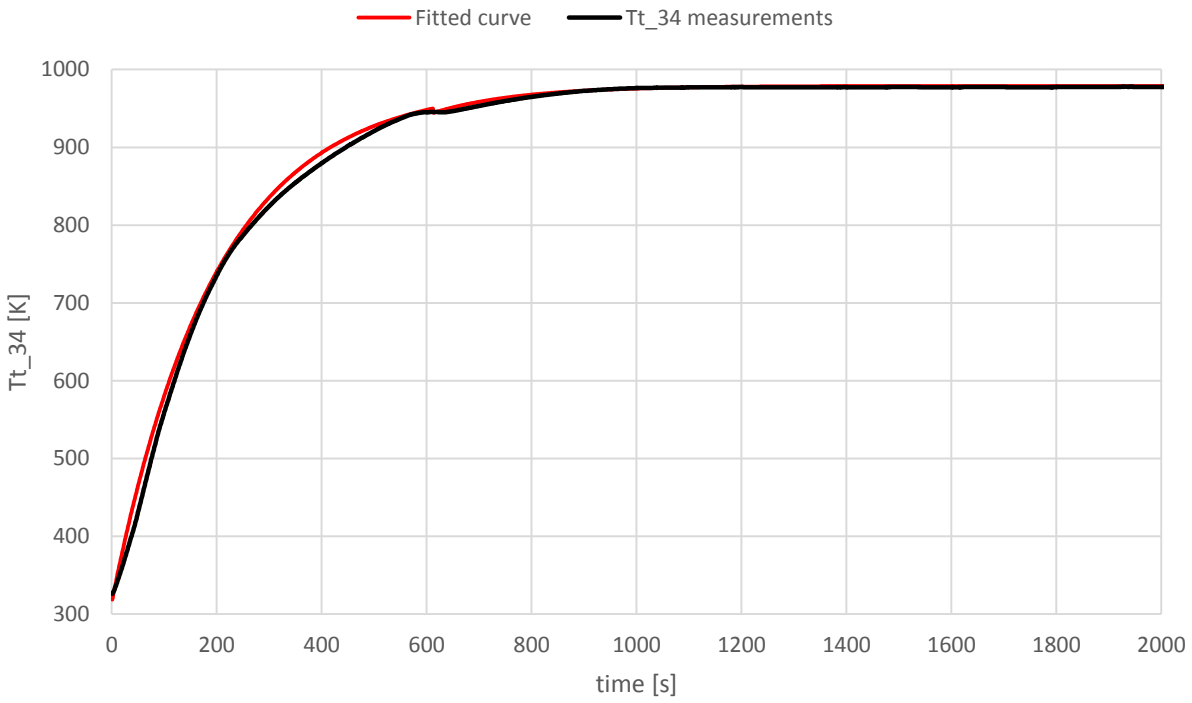

Figure 14 Results of curve fitting for Tt_34(t)

The maximum error between *Tt_34* and the fitted curve is around 34 K. Curve fitting established good results, although we were still concerned how to define the steady state of the system. A value of *Tt_34* should be stated that determines the steady state. The recuperator temperature fluctuates significantly even after smoothing the data by calculating the average of the nearest values, which is already producing some errors. Therefore, reaching a specific *Tt_34* value does not have to be the equivalent of reaching the steady state.

This is how we analyzed other parameters and searched for alternative methods to estimate energy production and consumption when starting the system.

3.2.3.2. Thermal energy calculations for the start

We assumed that fuel mass flow rate could be another parameter expected to show stability over time in steady state conditions. Figure 15 represents fuel mass flow rate over time, around 1300 s after of the cold start. It can be concluded that fuel mass flow rate does not expose stability for around 2500 s of the measurement. Therefore, the fuel mass flow rate cannot be considered as a reference parameter for defining the steady state condition of the system.

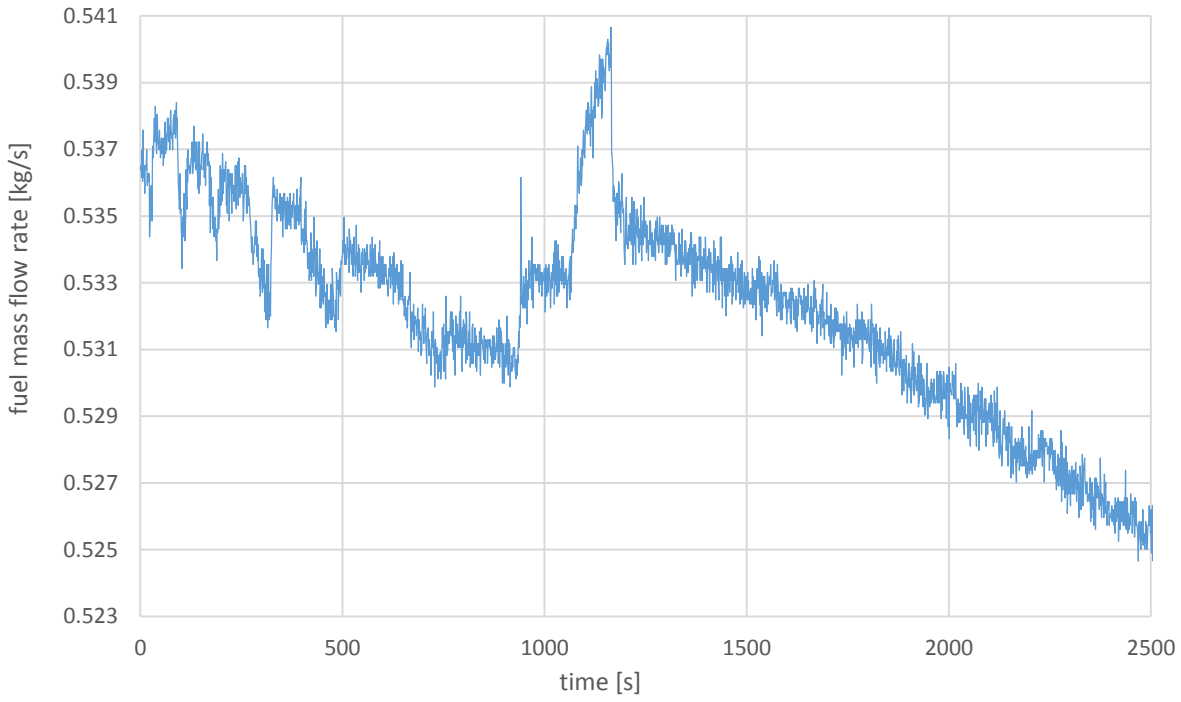

Figure 15 Fuel mass flow rate 1300 s after the start of the system

The processed data showed that thermal power could be a suitable parameter for defining the steady state. Thermal power is the result of the equation:

(6) $$P\_th = \dot{m}_w * c_p * \Delta T$$

Where:

P_th – is the thermal power [kW]

$\dot{m}_w$ – is the water mass flow rate [kg/s]

c_p – is the water specific heat capacity [kJ/kg K]

ΔT – is the temperature difference between the supply and return water temperature [K]

The water mass flow rate meter exhibits many fluctuations, but these fluctuations have a repetitive pattern and can be easily averaged. The averaged power increases constantly until steady state. Figure 16 represents the thermal power measurements (blue line) starting around 1700 s after a cold start at full load. The red dotted line is a trend line over thermal power values for more than 2100 s (about 35 min). The trend line is expressed by the function: P_th = 3E-08*t + 0.0039. The coefficient a = 3E-08 is significantly small, which indicates reaching a steady state of the system operation.

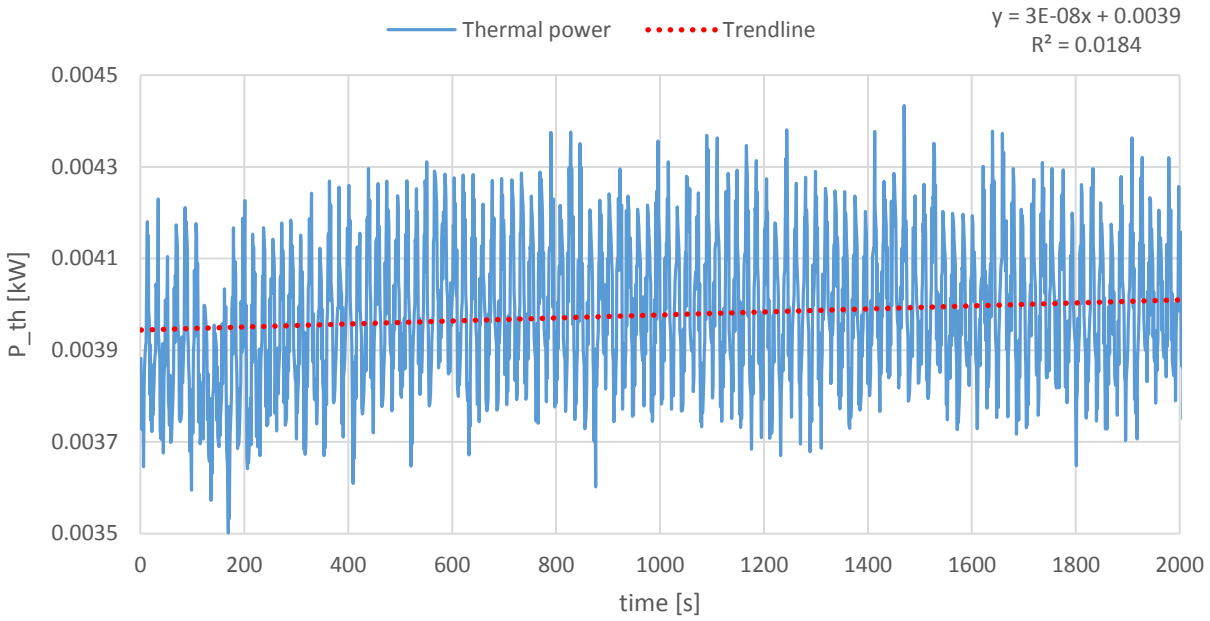

Figure 16 Thermal energy derivative after the 1700s from the moment of cold start at full load

The time to reach steady state depends on the system temperature *Tt_34_0* at the start. The warmer the system, the faster it reaches steady state. Experience showed that 1700 s is the minimum time for the system to reach steady state after a cold start. In all other tests, with higher initial *Tt_34_0*, the system reached steady state earlier. The considered time was increased from 1700 s to 2000 s to be sure that in slightly different external conditions (i.e. different outside temperature), steady state was reached, even with a cold start.

3.3. System modelling

This section presents the model of the system that describes the system performance. The model consists of the set of equations based on the experimental data and obtained in Excel and Python. Equations represent the relations between dependent variables: thermal, electric and fuel energy, and independent variables: time and the electric load. The system behavior differs in starting (heating up), steady state and cooling operation. Therefore, thermal, electric and fuel energy are described by different equations in each of these operating conditions. These equations were used to optimize the system performance in the next chapters.

3.3.1. Starting/heating up

In this dissertation for the purpose of modeling the system, starting (or heating up) of the system is referred as the operation of the system for the initial 2000 s. The produced thermal and electric energy and consumed fuel energy during this time depends on the load (set point – *SP*) and the recuperator temperature (*Tt_34_0*) at the start. Multiple regression analysis was used for modeling system starts with different beginning recuperator temperature and different loads.

Table 6 represents calculations of the electric, heat and fuel energy, 2000 s after the start of the tests, with various loads and initial recuperator temperatures. Energy values entail errors solely due to measurement inaccuracies of the devices.

Table 6 Electric, thermal and fuel energy calculations 2000 s after starting the system for various loads and initial recuperator temperatures

***SP* [%]**	***Tt_34_0* [K]**	***E_el* [kWh]**	***E_th* [kWh]**	***E_f* [kWh]**
100	**599**	1.551	8.358	11.394
100	**864**	1.664	9.075	11.062
80	**600**	1.250	7.024	8.451
60	**444**	0.774	5.049	8.378
60	**571**	0.882	5.355	8.444
60	**754**	0.865	5.761	7.840
40	**451**	0.635	4.388	7.808
40	**628**	0.675	5.147	7.531
40	**738**	0.629	5.316	6.822
40	**872**	0.650	5.479	6.620
20	**444**	0.448	3.723	7.313
20	**762**	0.484	4.662	6.091

The next step was to obtain equations that allow calculating the electric, thermal and fuel energy for any value of *SP* and *Tt_34_0*.

Equation (7) represents a polynomial regression equation with two independent variables x_1 and x_2.

(7) $$y = \beta_0 + \beta_1 x_1 + \beta_2 x_2 + \beta_{11} x_1^2 + \beta_{22} x_2^2 + \beta_{12} x_1 x_2$$

The graphical representation of this equation is a surface whose shape depends on the coefficients: $\beta_0, \beta_1, \beta_2, \beta_{11}, \beta_{22}$ and β_{12}. In 3D, the surface edges can have different forms, i.e. parallel, ellipses, and

parabolas. The independent variables x_1 and x_2 correspond to the *SP* and *Tt_34_0* and the dependent variable is E_i, where i= {el, th, f}.

(8) $$E_i = \beta_0 + \beta_1 * SP + \beta_2 * Tt_{34_0} + \beta_{11} * SP^2 + \beta_{22} Tt_{34_0}{}^2 + \beta_{12} * SP * Tt\_34\_0$$

The difficulty was to find coefficients of Equation (8) to fit the set of data from the Table 6. Coefficients were obtained by a surface fitting to the energy values with the least squares method. Scientific Library for Python (SciPy) is a collection of numerical algorithms and toolboxes including optimization. Scipy.linalg toolbox helps to implement the least squares algorithm. The results of the optimization are three sets of coefficients for Equation (8) that create three polynomial functions for the electric, thermal and fuel energy, respectively. In Figure 17, Figure 18 and Figure 19 the data from the Table 6 are plotted in three dimensions along with the fitted functions to check for the adequacy of the fit. In Figure 17, 18, 19 red dots represent the measured energy values for corresponding recuperator initial temperatures and loads.

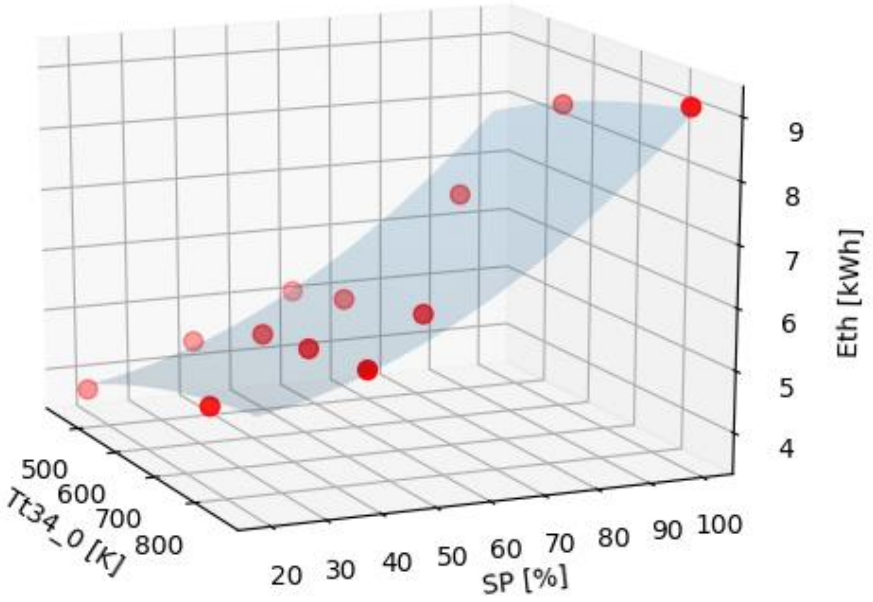

Figure 17 Surface fitting for thermal energy values for different Tt34_0 and SP.

Figure 17 represents the results of the surface fitting for thermal energy values calculated for the 2000 s after the start of the system at different loads and initial recuperator temperatures. Equation (9) displays the system model for thermal energy calculation at the start of the system.

(9) $$Eth = -3.4E\text{-}6 * Tt34_0{}^2 + 4.5E\text{-}4 * SP^2 + 3.4E\text{-}6 * Tt34_0 * SP + 7E\text{-}3 * Tt34_0 - 6E\text{-}3 * SP + 1.3$$

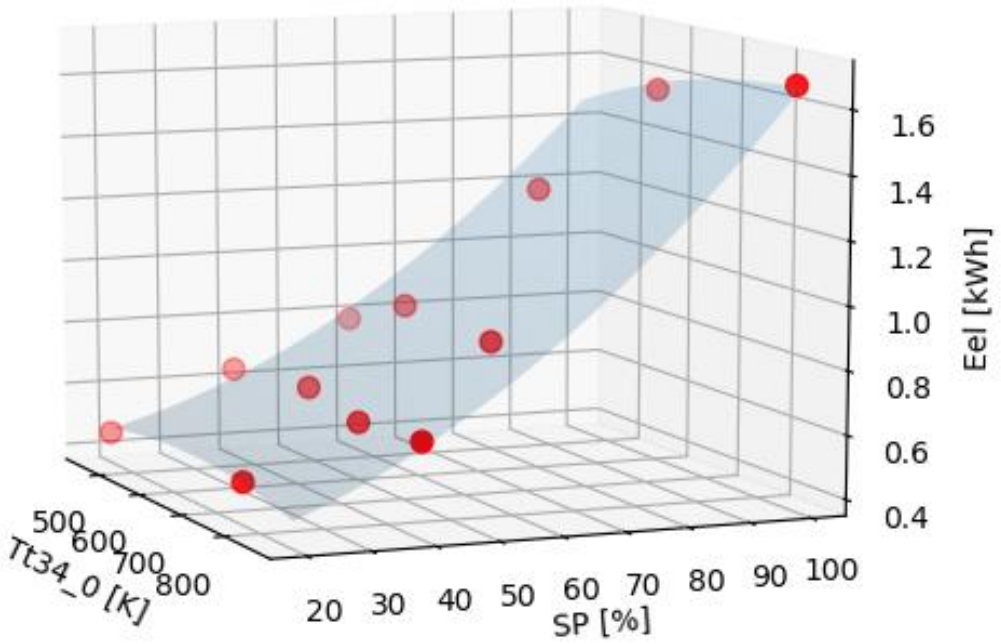

Figure 18 Surface fitting for electric energy values for different Tt34_0 and SP

Figure 18 represents calculated fuel energy for the steady state achieved 2000 s after the start with different load and initial recuperator temperature, and the surface that fits these values. Equation (10) displays the coefficients of the fitted surface.

(10) $Eel = -E\text{-}6 * Tt34_0^2 + 9.4E\text{-}05 * SP^2 + 6.6E\text{-}6 * Tt34_0 * SP + 1.1E\text{-}3 * Tt34_0 - 1.7E\text{-}3 * SP + 8.7E\text{-}2$

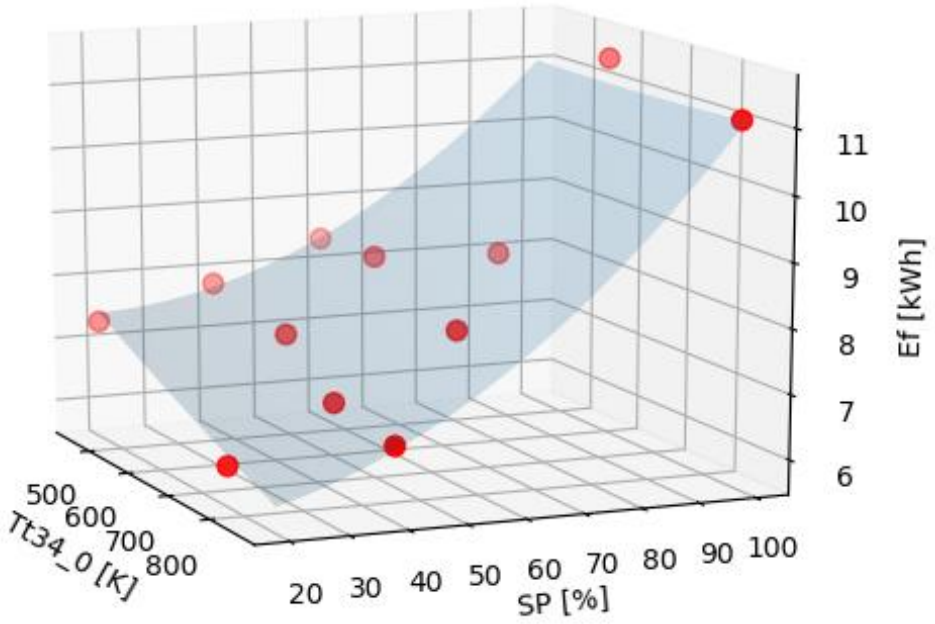

Figure 19 Surface fitting for fuel energy values for different Tt34_0 and SP

Figure 19 represents fuel energy values calculated for the 2000 s after the start of the system at different loads and initial recuperator temperatures and surface that fits these values. Equation (11) displays the coefficients of the fitting surface.

$$(11)\quad Eel = -8.5E\text{-}7 * Tt34_0{}^2 + 5.2E\text{-}4 * PC^2 + 4.7E\text{-}5 * Tt34_0 * PC - 5.7E\text{-}3 * Tt34_0 + 3.9E\text{-}2 * PC + 10$$

3.3.2. Steady state

Produced thermal and electric power, and consumed fuel power during the steady state operation depends on the load. The higher the load, the higher value of the thermal, electric and fuel power. Cumulative thermal, electric or fuel energy produced is the integral of instantaneous thermal, electric or fuel power, respectively. Obviously, energy increases proportionally with the operational time. Therefore, each of the mentioned above energies in steady state conditions can be expressed as a function of two independent variables: the set point and time.

The net electric efficiency and the total energy efficiency do not decrease linearly with a decrease of the set point due to the nonlinear decline of electric power. The decreasing rate for electric output is smaller for the *SP*s higher than 60%. Efficiencies follow the same pattern. The recuperator temperature increases with the decrease of the load (set point), to reach more than 1000 K at the minimum, *SP*=20%.

Figure 20 represents the system input and output at different loads. Larger dots display values of the electric, thermal and fuel power as a function of the set point. Dotted curves are the best fit for the series of the thermal, electric and fuel energy data. Constructed functions are second order polynomials. The differences between measured energy values and energy values calculated with the fitted functions are less than 5%. The highest relative error, of about 4.5%, is for the thermal energy value at *SP* = 60%. This can be considered as a marginal error and proves that the fitting is suitable. As an outcome of this model, there are three quadratic functions: *P_el(SP)*, *P_th(SP)* and *P_f(SP)* for the heat, electric and fuel power, respectively, that contain one independent variable – set point.

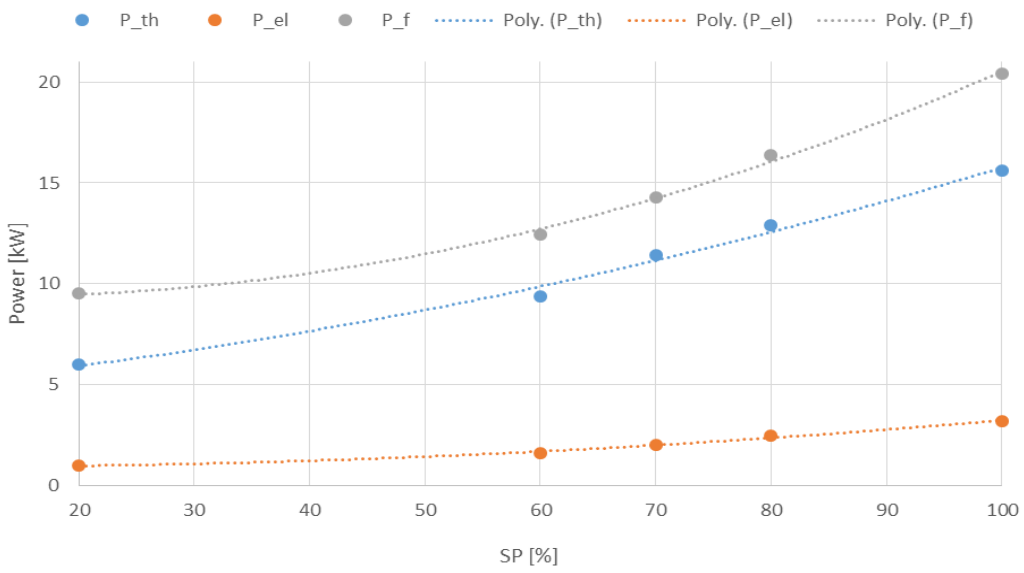

Figure 20 Powers at different loads

The electric, thermal and fuel power in steady state operation is considered to be a constant that depends on the set point. Therefore, the electric, thermal and fuel energy can be calculated by the following equation:

(12) $$E_i = P_i(SP) * t$$

Where:

P_i (*SP*) – is a quadratic function of the instantaneous power input or output of the system operation in steady state condition;
i – is the index that denotes the electric, thermal and fuel power *i* = {*el, the, f*};
t – is the time of the system operation in the steady state.
Equation (12) is a second order function of *SP* and a linear function of *t*.

3.3.3. Stopping and cooling down

The set point is selected to 0% in the control panel to stop the system. It takes around 2 min to reduce the speed of the engine to 0 rpm, for an operation at full load. During this time, the system continues to extract thermal and electric power at a smaller rate, but the overall energy production is not much greater than the measurements' error. However, we decided to include the impact of these energies on the system performance to make the optimization model more representative. The thermal and electric energy produced while the engine slows down are considered equal for all loads and independent of the external conditions. The thermal energy is around 0.455 kWh and the electric energy is around 0.011 kWh.

When the speed of the engine is reduced to 0 rpm, the system is still hot enough to heat the circulating water and produce a further small amount of thermal energy. While the recuperator temperature is above 812 K, i.e., approximately for the first 2350 s, the water pump runs periodically for 6 s, once every 55 s. The

pump operates less frequently after that and stops completely (and there is no more increase of the thermal energy) when the recuperator temperature drops to around 650 K; this happens around 9007 s after the engine came to a stop. Figure 21 represents the thermal energy produced while cooling down the system after the engine stopped. This thermal energy function can be fitted to two linear functions with different steepness in two time ranges, the first one where 0 s ≤ t ≤ 2350 s and the second one where 2350 s < t ≤ 9007 s.

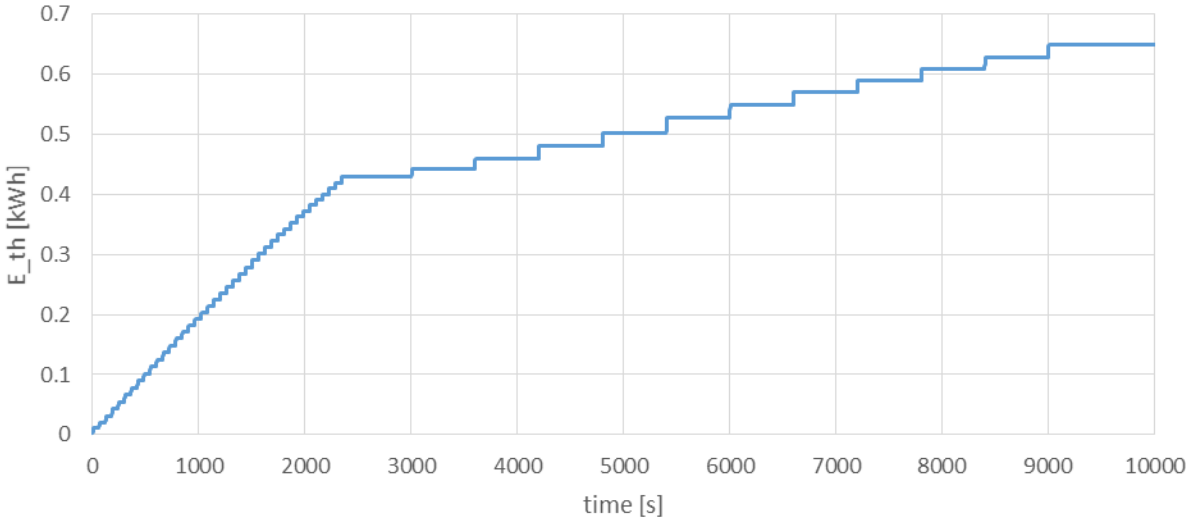

Figure 21 Accumulated heat production during cooling down of the system

Figure 22 represents the thermal energy produced in the first range of time (blue curve). The red dotted line is a linear approximation of the energy function. The relative error between the measured thermal energy and the fitted function is less than 1.5%.

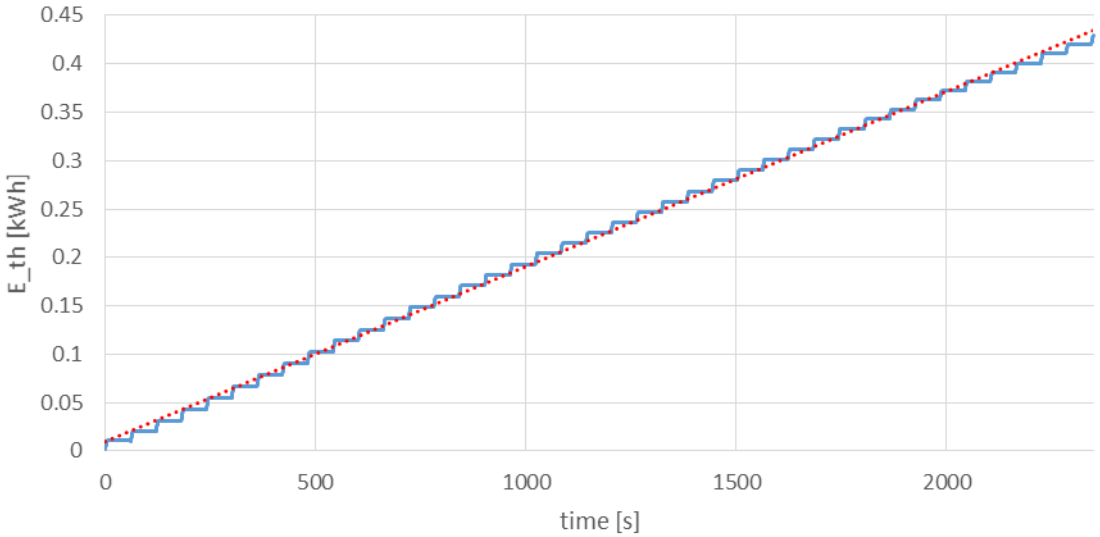

Figure 22 Thermal energy up to 2350 s after stopping the engine

The blue curve in Figure 23 represents the thermal energy production when cooling down the system in the second time range (2350 s < t ≤ 9007 s). The red dotted line is the linear approximation of that energy function in this time interval.

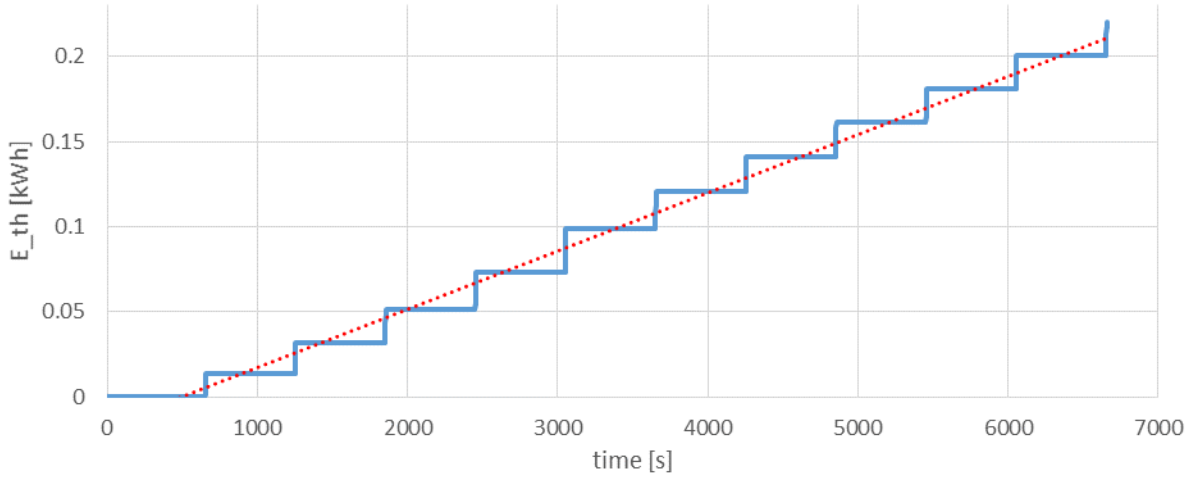

Figure 23 Thermal energy after about 2350 s from the moment of stopping the engine to about 6500 s

There is still some electricity consumed by the electronic control and the pump during these two cooling down stages. The cabinet ventilator also works when the cabinet temperature is too high. From the Figure 24, it is seen that the electric energy can be approximated by a second-degree polynomial.

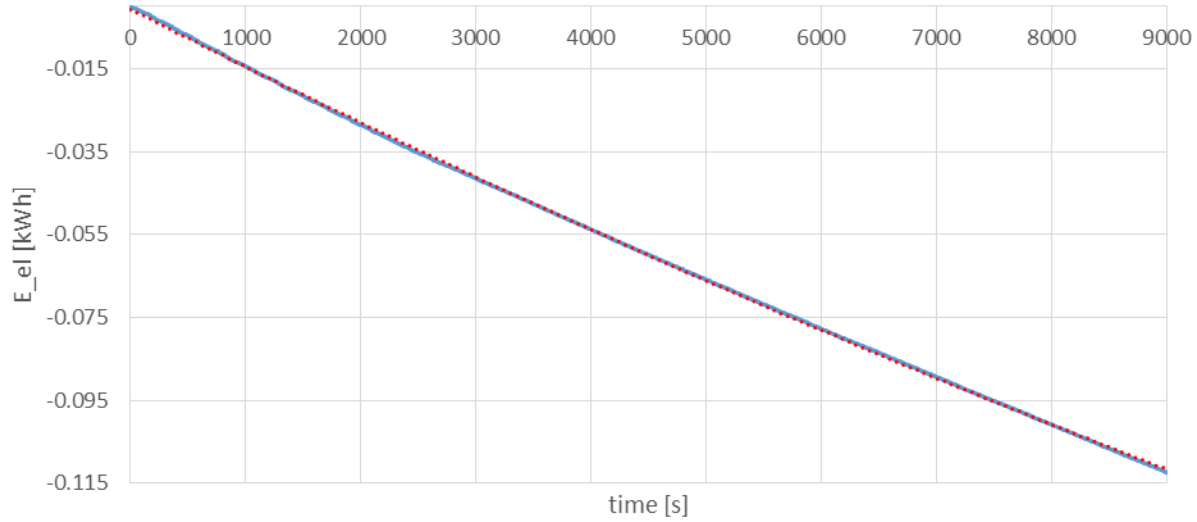

Figure 24 Electricity consumed during cooling down the system

4. Optimization numerical model

4.1. Buffer vessel implementation

4.1.1. Buffer vessel basic assumptions

Energy storage comprehends a wide range of technologies, according to the amount of energy at stake, the particular application and the size of the power plant. Energy can be stored as electrical, chemical, potential, kinetic or thermal energy. In a thermal energy storage (TES) tank, heat can be used directly. Systems based on the sensible heat capacity of the storage material, like hot water tanks, are examples of this technology. Storing heat in hot water is a well-established practice and is used in the full range of energetic capacities. The design of these systems must consider stratification, the trade-off between heat loss and storage temperature and the trade-off between longer-term storage and the insulation cost [18].

In the numerical model developed along these pages, the micro-CHP system with TES will be used in one case only for sanitary hot water (SHW) and, in the second case, for domestic hot water and space heating. This model does not include the plate heat exchanger (number 11 in **Error! Reference source not found.**4), the water pump (number 10 in Figure 4), water temperature and flow sensors, valve and a radiator. The only heat control parameter of the MTT buffer vessel is the buffer vessel temperature (number 2 in Figure 4). For the sake of simplicity, the numerical model assumes a direct energy extraction from the vessel, not considering pumps, heat exchangers and the response of other sensors.

4.1.2. Buffer vessel sizing

Choosing the appropriate size for the buffer vessel for a CHP system is a very complicated task; there can be several methods. The internal volume of the system filled with water already provides some amount of storage. Therefore, for a given temperature difference,

(13) *storage design capacity = (required system volume) – (actual system volume)*

Where:
Required system volume – is the necessary system output to accommodate the demand
Actual system volume – is the water volume in all pipes and heat exchangers.

There are critical issues that should be addressed when applying a micro-CHP or any other heat plant with thermal storage. Undersized buffer vessels are inefficient because they will not capture sufficient heat from the thermal unit to meet the demand. On the other hand, the oversized thermal storage systems have a higher investment cost, possibly a higher maintenance cost, a higher heating up time and it is subject to higher losses, given their bigger surface area [19].

To accurately define the size of a thermal storage for CHP system, it is necessary to make a series of calculations for different storage sizes with the heat demand, preferably using steps of one hour for the whole year.

In [20] there are two commonly recognized approaches for the TES modeling.

a) Simplified approach

It is extensively used since the 1980's. Recently in [21], applied this TES modeling approach to the optimal control strategy of the micro-cogeneration system in residential applications. The storage tank is assumed to have a constant volume (of cylindrical shape, in most cases), a homogeneous water temperature, an instant mixture of flows in the tank and negligible radiation losses. Heat losses are described by the equation:

(14) $$Q_{loss} = A * h * \Delta T = A * h * (T_{storage} - T_{env})$$

Where:

A – is the buffer vessel surface area $[\mathrm{m}^2]$

h – is the heat transfer coefficient [W /(m^2 K)]

$T_{storage}$ – is the uniform temperature of the storage material [K]

T_{env} – is the ambient temperature [K]

b) Stratified storage model

In this model, the storage tank is divided into a few layers. There are ready-made software applications, like TRNSYS, to handle the calculations of these models. For each layer, the heat balance is calculated with the mass entering from below and exiting above the layer; heat conduction between the layers and heat losses to the environment are evaluated. In our real EnerTwin application, a buffer vessel relying on thermal layering would result in a higher temperature of the water layer at the top than at the bottom, due to the water density difference. High water flow rates should not occur, to prevent turbulence from compromising stratification.

The best evaluation of the real TES operation and especially of its losses lays somewhere in between both approaches. We only used the simplified approach, with homogenous temperature, since stratification is always partial and is not yet a standard widely spread technique. It was assumed that the minimum volume of the storage tank was 800 liters, a requirement of German subsidies – the main market of the MTT sales strategy.

The buffer vessel volume is one of the input parameters for the optimization model. The buffer vessel surface area is used to calculate the heat losses of the buffer vessel according to the Equation (14). It is assumed that the buffer vessel has a cylindrical shape. Figure 25 represents the buffer vessel drawing with its main dimensions.

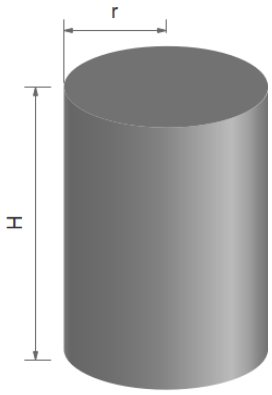

Figure 25 Buffer vessel sizing

(15) $$A = 2\,\pi\,r\,H + 2\,\pi\,r^2$$

(16) $$V = \pi r^2\,H$$

Equations (15) and (16) represent calculations of the buffer vessel surface area and volume with the generic dimensions of Figure 25.

4.1.3. Buffer vessel losses

Figure 26 and Figure 27 illustrate the buffer vessel losses for different storage sizes and different storage temperatures. These values were calculated from Equations (14), (15) and (16). The maximum storage temperature defines the maximum load of the buffer vessel. Figure 26 illustrates an increase in heat losses with bigger storage surface area, while Figure 27 compares the heat losses for different volumes of the storage tank. Calculations and visualizations were made in Python using Python's modules and algorithms with the following assumptions:

- environmental temperature T_{env} = 20 °C,
- thermal conductivity of the insulation material (polyurethane foam):
  λ = 0.03 W/(m K) [22],
- insulation thickness s = 0.1m,
- heat transfer coefficient:

(17) $$\frac{\lambda}{s} = \frac{0.03}{0.1} = 0.3\ \frac{W}{m^2\,K}$$

- radius and height of the cylinder, varying between defined minimum and maximum:

(18) $$0.25\ m \leq r \leq 2\ m$$

(19) $$0.5\ m \leq H \leq 3\ m$$

The results are presented as a function of the surface area and volume of the buffer vessel.

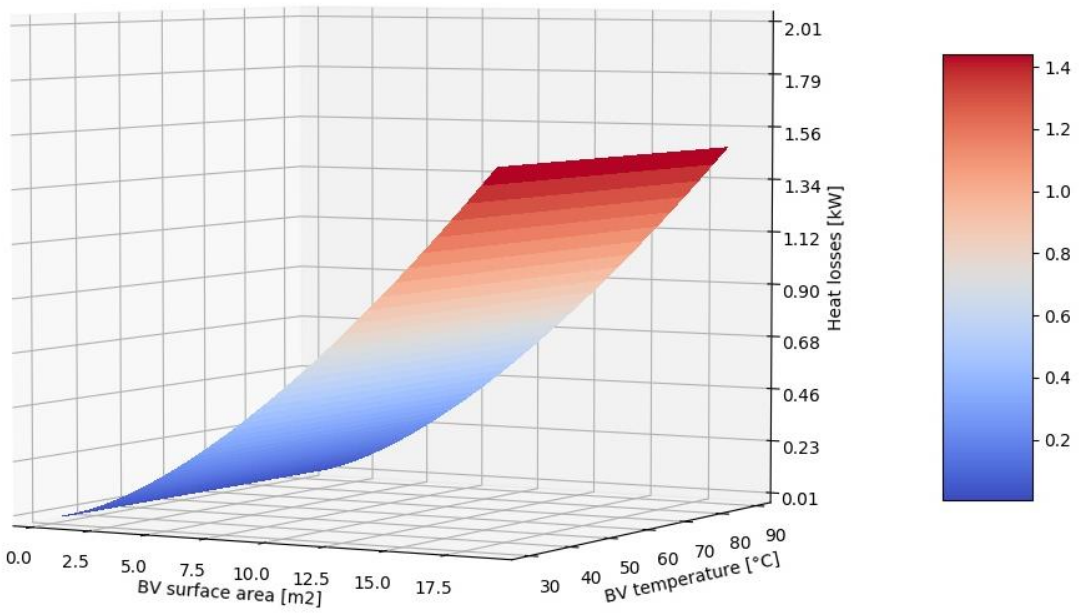

Figure 26 Buffer vessel losses for different dimensions and different storage water temperatures

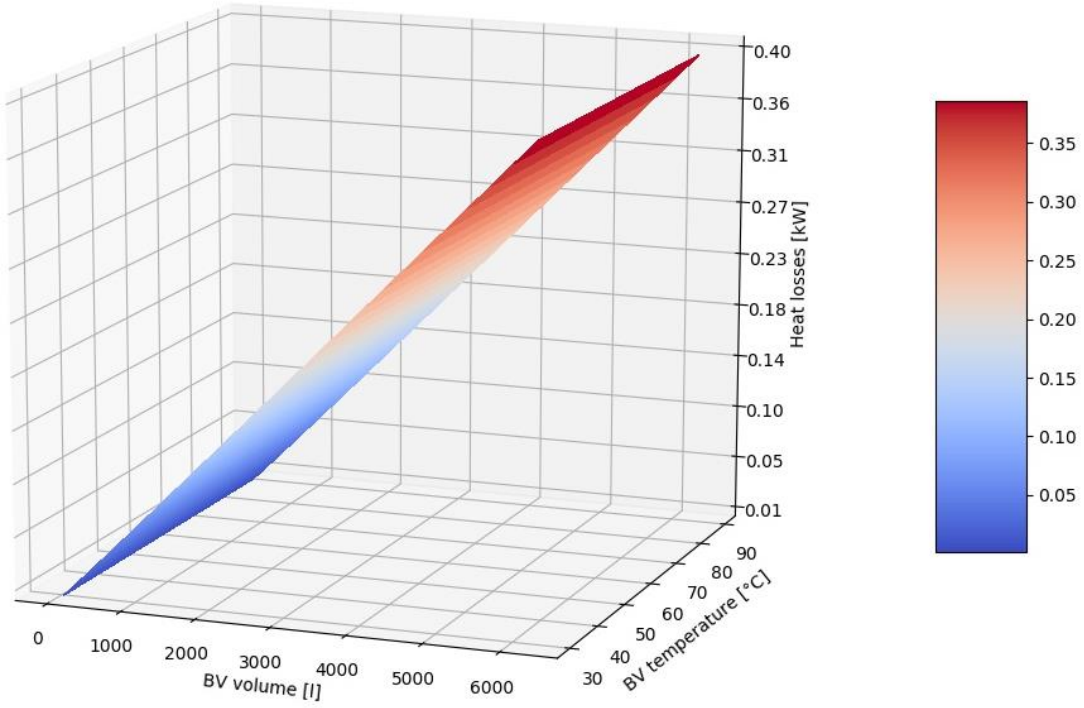

Figure 27 Buffer vessel losses for different volumes and different storage water temperatures

A given cylindrical volume can have different sizes and, therefore, different surface areas. In order to minimize the heat losses, the buffer vessel surface area should be a minimum for the required volume. Ideally, the smallest surface area occurs for an infinity long cylindrical shape of the buffer vessel. Thus, we have to implement constraints for the minimum radius of the BV.

Minimize {$A(H, r)$}

Where:

$A(H, r)$ — is the objective function of the buffer vessel surface area to be minimized

Subject to:

(20) $$r > 0.2\ m$$

(21) $$0.2\ m < H < 2\ m$$

(22) $$V \geq 0.8\ m^3$$

We have a minimization code in Python to evaluate the surface area of the buffer vessel, knowing the required buffer vessel volume and the constraints (as stated above).

4.2. Assumptions

The optimum operating profile needs to be determined to maximize the efficiency while complying with the heat demand. The concept of the optimization of the micro-CHP was to prove if it is worth to run the system at part load. Operation in part load and transient state, in a start/stop mode, is characterized by a smaller efficiency than at full load operation. When the system is equipped with a buffer vessel, its operation can be controlled by the temperature of the water inside the tank as explained in section 4.4. As a result, this control implementation leads to forced start and stop of the system when the required buffer vessel temperature is reached. The numerical model should optimize the decision regarding how to operate the system, depending on the heat demand profile of the user and the TES size. The daily heat demand profile is discretized in time intervals bigger than 2000 s, which is the minimum time required for starting. The optimization algorithm has to make an optimal decision in every interval (every 2000 s) knowing the state of the system during the previous interval. The options to be chosen are listed below:

1. At the time being, the system is not operating.
   In the next step:
   a) The system should remain stopped.
   b) The system should start operating.
2. At the time being, the system is operating.
   In the next step:
   a) The system should remain operating.
   b) The system should stop operating.

We assume that at the beginning of the first interval, at time $t = 0$, the system is not operating and is cooled down to the environmental temperature, so that the recuperator temperature is approximately *Tt_34_0* = 300 K, but the buffer vessel is already fully loaded at its maximum temperature *Tbuf_max*. In subsequent time intervals of 2000 s, it may occur that *Tbuf_max* is exceeded because the control algorithm only checks the temperature every 2000 s. In order to avoid completely exceeding the limit, the control model should run continuously, checking the temperature continuously.

The function to be minimized is the economic value of the fuel consumed, subtracted from the economic value of the electricity produced. The feed-in-tariff of electric energy and the cost of natural gas are widely volatile and therefore difficult to predict. The rates of electricity and gas in Europe are specific for each country and vary according to the individual contract of the end-user (for example, depending on the amount of energy consumed). Taxes also influence the energy prices and vary from one region to another. In this work, energy prices for the German market from 2016 were used. The natural gas price is equal to 0.064 EUR/kWh [23]. The value of the electricity produced is calculated as the sum of the electricity price for household consumers 0.298 EUR/kWh [24] and subsidy bonus of 0.6 cents/kWh [25]. Evidently, the relative difference in the price of gas and electricity is a natural economic driver for the profitability of micro-CHP units running on natural gas.

4.3. Heat demand profile

For the simulation of the model, a heat demand profile is needed. The MTT company itself does not acquire such data, thus, it had to be generated from an external source. Generally, the heat demand profile is necessary for the sizing of the power generation source.

Users' heat demand profile is chosen for the German latitude since it is the main target market of MTT.

In 2013, in Germany, 28% of the total final energy stood for the residential sector, which highlights its importance in terms of the environmental protection. Most of the residential energy is allocated to space heating. In 2013, in Germany, around 70% of the total energy in the residential sector was used for space heating, while 13% for sanitary hot water and the remaining 17% accounted for electric applications [26]. Stricter EU regulations concerning building energy efficiency and the introduction of renewables in the energy shares are encouraging researchers to develop more accurate thermal user's profiles. In [26] there are four main methods for calculating the load profile.

- One is to use average load profiles, often referred to the outside temperature. The drawback of this approach is that these average profiles do not reflect variations due to personal requirements.
- The second method uses a reference load profile, selected from the set of profiles for that specific outdoor temperature, weather conditions and weekday. The disadvantage of this method is that only a finite number of profiles are selected.

- The statistical method is based on measured data compiled, for example, by a regression analysis. Some limitations occur when applying the method to a new building or when the dynamics of the system change.
- The fourth method is a more physical approach. It uses the energy balance equations with the physical data of the specific building. Unfortunately, this approach cannot reflect the human behavioral reactions to the heating profile. The author in [26] applies a combined physical and behavioral model. Sanitary hot water usage, for instance, is strongly dependent on the users' social and economic circumstances. The calculations are based on a survey and then they are validated with measurements. As a result, an average sanitary hot water profile represents the set of profiles of family houses in different regions in Germany in different seasons. The paper also considers the average space heating demand profile, with assumptions similar to those of the SHW profile. These two profiles are presented in Figure 28 and Figure 29.

As mentioned previously, the time interval for taking control decisions is 2000 s, thus for the 24 h, there are 44 time intervals, where the last time step is shorter than 200 s – 400 s. For each time step, there is a different heat power. All the 44 points are joint with one line. The two profiles for SHW and space heating are merged together as shown in Figure 30.

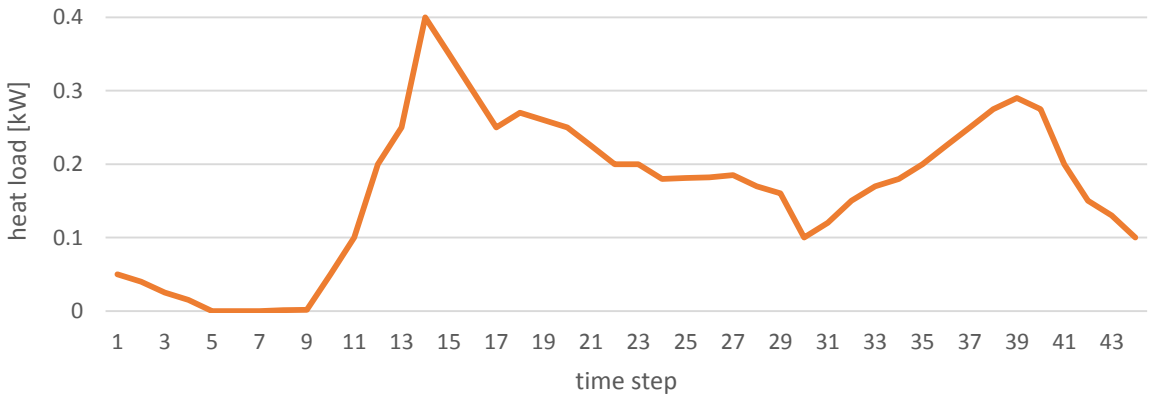

Figure 28 Average daily SHW demand profile

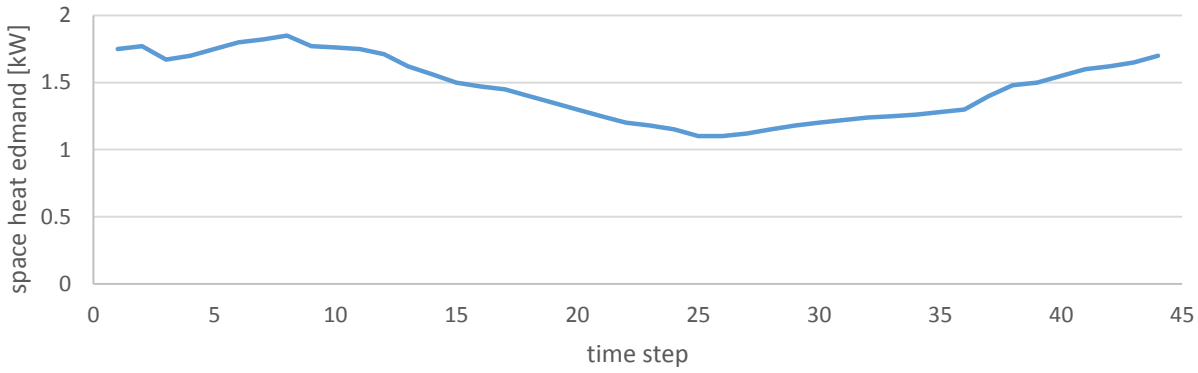

Figure 29 Average space heat demand profile

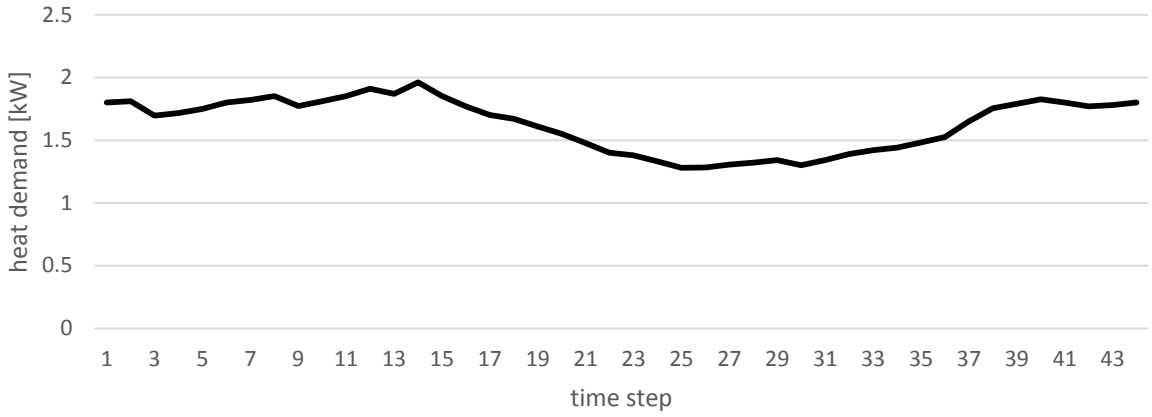

Figure 30 Merged heat demand profile for SHW and space heating

There are two cases implemented in the performance optimization model of micro-CHP. The first one, when the system is producing heat only for the purposes of sanitary hot water, and the second case when the heat is demanded for both SHW and space heating. The heat demand data shown in figures above, presented too low values for the optimization model, as the algorithm could not determine an optimum operation for a profile based on such data. Thus, the heat demand value of the heat was multiplied. What is important is that the proportion and the pattern of data are preserved.

4.4. Mathematical system formulation

When there are several decisions to be made and some of them influence others, the general strategy should optimize the whole system. One way of doing this is to optimize subsystem inside a global optimization loop. The techniques used in dynamic programming consist of a combination of well-known algorithms: linear, integer, quadratic and nonlinear programming [27].

To be able to optimize the operational control of the micro-CHP we chose the minimization of the overall running cost as target function. The complete Python programs can be seen in Appendix A. A separate

Python file (Appendix B) includes the functions describing the thermal energy and electricity production, and fuel energy consumption when starting, in steady-state conditions and when cooling down.

Firstly, the constant parameters are defined, namely, the produced thermal energy and electricity during stopping (*Eth_stopping* and *Eel_stopping*) and time *tstopping* spent to decrease the speed of the engine to 0 rpm.
Next, some physical parameters are introduced, namely:
Cp – water specific heat capacity;
U – overall heat transfer coefficient (only the conduction across insulation is relevant) used to calculate heat lost to the environment
The control of this system is programmed to take decisions regarding the system's state (running or stopping) only at fixed time intervals. The smallest time interval available is 2000 s and therefore we chose this value since it provides the more refined control possible. Therefore, variable *time_interval* is set to 2000. As mentioned, the total simulation time is 24 h and hence the value number of the interval is *time_steps* = 44. The heat demand profile *load* is introduced as an array of *time_steps* items.

The buffer vessel volume *V_init* has a minimum value of 800 liters. Given that, the buffer vessel surface area *A* is calculated by minimization as described previously with a least squares Python algorithm from the module SciPy.

Other parameters introduced are:

Tenv – is the environment temperature
T0 – is the initial buffer vessel temperature
TB_max – is the set point temperature of the buffer vessel. When it is reached, system should not be providing more heat to the buffer vessel
TB_min – is the trigger point temperature of the buffer vessel. When it is reached, system should be providing heat to the buffer vessel
B0 – is the initial buffer vessel capacity
Bmax – is the maximum buffer vessel capacity
Bmin – is the minimum buffer vessel capacity
N_eval – is the number of permitted function evaluations
V – is the buffer vessel volume

The maximum buffer vessel capacity is calculated as:

(23) $$Bmax = V * (TB\_max - T0) * Cp$$

The minimum buffer vessel capacity is calculated as:

(24) $$Bmin = V * (TB\_max - TB\_min) * Cp$$

Variable *binary* indicates whether the system is operating at full load or part load. *Binary* can take values True or False. If the value is True, it means the system is either at *SP* = 100% or it is not operating. When the value is False, the *SP* can take any value between 0% and 100%, but from 0% to 20% the control algorithm will not let the system operate.

The meaningful values of *SP* are in the range [0, 100]. However, *SP* values are generated randomly and we wanted to have an equal probability of having the system operating or not. Therefore, the bounds for the random *SP* are [-60, 100]. In this fashion, the probability of operating the system is the same as the probability of not operating it, since only *SP* higher or equal to 20 make it operate.

The objective of the optimization is to minimize the overall cost-function described by:

(25) $$Cost = \Sigma_i^{time\_steps}[- E\_el \ (p\_el\_buy + p\_el\_sub) + E\_f * p\_f]$$

Where:

E_el – is the electric energy (in kWh) produced during time step *i*

p_el_buy – is the price of electricity (€/kWh) in Germany

p_el_sub – is the amount of subsidies (€/kWh) for the production of electricity in micro-CHP

E_f – is the fuel energy (kWh) consumed during time step *i*

p_f – is the price (€/kWh) of the natural gas energy

Note: the minimum of a function f(x) is the maximum of the function –f(x). Therefore, the maximization of a function can be performed as the minimization of the negative of that function (Figure 31).

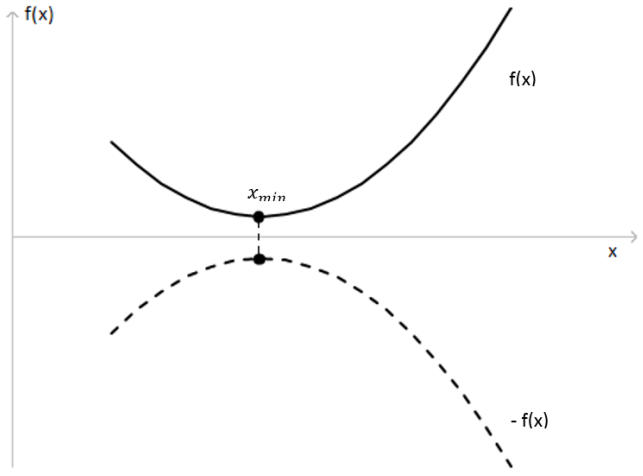

Figure 31 Minimum and maximum of a function

Then, the maximum can be found by searching for the minimum of the negative f(x) and then changing the sign of the function. For practical reasons, this has been done in the algorithm and that is why a minus sign appears in function Electricity since max[f(x)] = −min[−f(x)]. Electricity has negative notation in Equation (25), since max[f(x)] = −min[−f(x)].

Figure 32 presents the flowchart of the system algorithm with its looping structure.

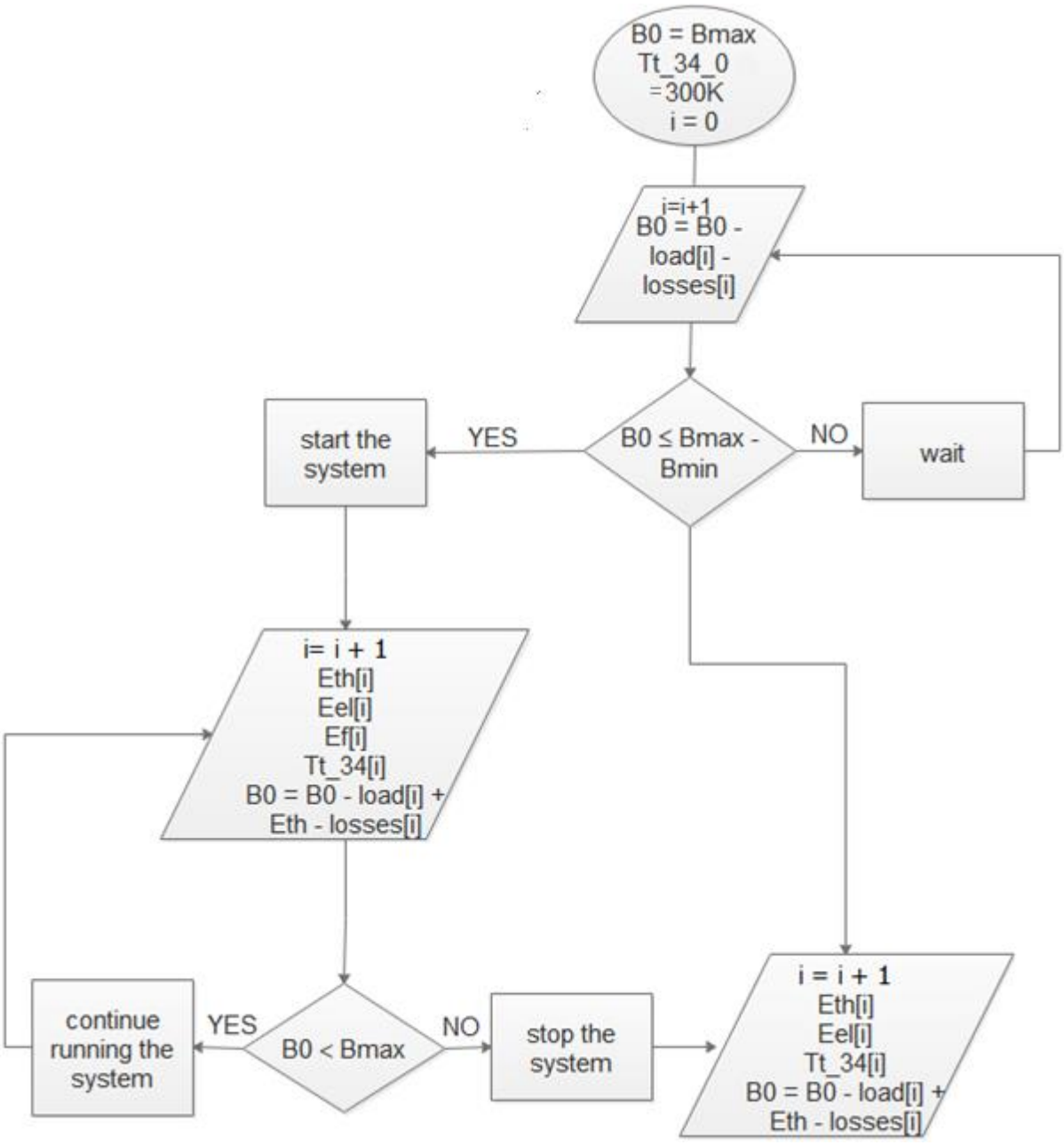

Figure 32 Flowchart of the system control algorithm

5. Simulation outcome and discussion

The section below presents results of the simulations of the system operation that has to comply with the heat demand. There are two different heat loads considered. One of them consists of the demand for the space heating and sanitary hot water, while the other covers the demand only for sanitary hot water, but for the larger scale. These load profiles are based on the profiles discussed previously but they had to be scaled up (simply by multiplication). The values of powers in profiles had to be increased because the system has too high capacity to comply with such a small demand and would have to operate significantly less frequently. The installation of the system for such demands would not be reasonable. However, the discussed heat demand profiles were still used to preserve the pattern of the heat demand profile. Furthermore, two different heat demand profiles (for the SHW and space heating and for SHW only) were used because the profile for the demand of sanitary hot water only contains some zero values, while the space heating demand is always greater than zero in the discussed profile. This can establish the behavior of the system in two different conditions. For each of the two heat demand profiles, the numerical model scheduled the operation of the system in two regimes. The first regime assumes operation only in a full load. There, the system can be in each interval only in two states: full load (*SP* = 100%) or inoperative (*SP* = 0). The other regime established in simulations for both types of heat demand profiles is when the system operates at a part load. Thus, its operation can have two status: operate in part load (*SP* < 100%) or inoperative (*SP* = 0%).

Below summarized setting for the simulation of the numerical model is presented:

- the buffer vessel volume *V* = 800 l
- the initial buffer vessel capacity is maximum
- the number of permitted function evaluations *N_eval* = 100 000
- two heat demand profiles are considered: for SHW, and for SHW and space heating together
- electricity prices and subsidies, and fuel prices as discussed in paragraph 4.2
- *time_interval* = 2000 s
- *TB_max* = 353.15 K
- The overall time covered by simulation of the system is 24 h
- buffer vessel heat losses are as discussed in paragraph 4.1.2.

5.1. Results for SHW and space heating

5.1.1. Operation at full load

Figure 33 presents the outcome of the numerical model simulation for the heat demand profile covering space heating and heat for sanitary hot water. In this first simulation, it was assumed that the system can operate only in full load. Thus all the black columns on the Figure 33 representing the set point (the load of

the system) have the value of *SP* = 100%. In the code, it is reflected by the value of the variable *Binary* equal to *True*. The orange line represents the heat demand profile with the value of the required heat power in each interval on the secondary axis. As stated previously, the initial buffer vessel capacity is maximum. Therefore, according to the simulation, the system does not have to operate in the very first intervals, even though there is already heat demand. With the time, the capacity of the buffer vessel decreases, until the minimum capacity is reached and so the system should start operating. When the buffer vessel reaches its maximum capacity, the system should stop. The logic is repeated further on. In each interval, we calculate the electrical and heat energy production as well as the fuel energy consumption. The simulation produced two system operation states, represented in Figure 33 by the set point values (in this case 0 or 100). There are 11 bars, which means that the system should be started 11 times. The second output of the numerical model are the values of the total electrical and the total fuel energy, produced and consumed, respectively, during the 24 h period. The total electrical energy and the total fuel energy is calculated as the sum of the electrical and fuel energy output in each interval, respectively. The third result of the simulation is the value of the objective function. The objective function that was minimized is the overall economic cost of the consumption of fuel, subtracting the overall economic cost of the extracted electrical energy (see Equation (25)).

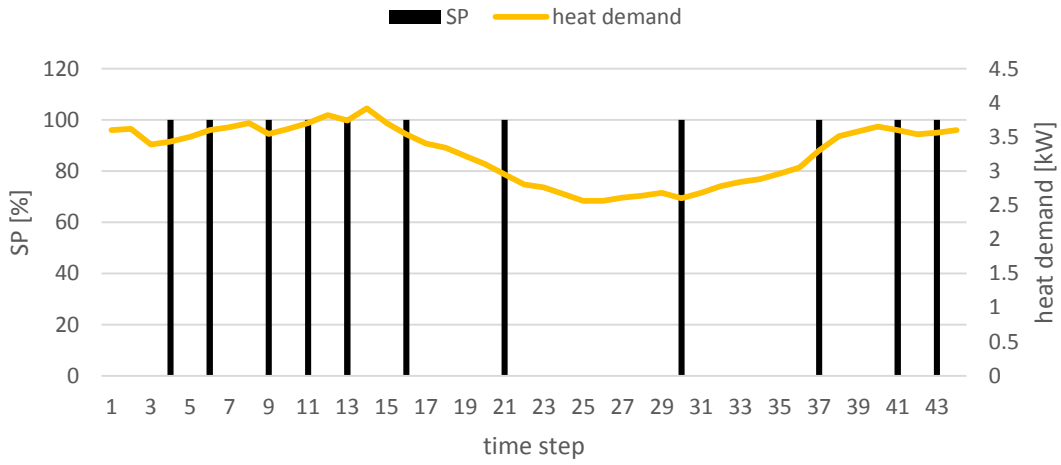

Figure 33 Simulated operating schedule of the system operations in full load with restriction to the total heat demand

5.1.2. Operation at part load

Figure 34 represents results of the simulation of the numerical model with the assumption that the system operates at part load to comply with the heat demand profile when the heat required is for sanitary hot water and space heating. The black columns represent the value of the set point that corresponds to the part load of the system. The number of bars corresponds to the number of starts of the system and it is higher (15 starts) than for the first simulation with a full load. The orange line represents the heat demand profile with

its heat power values on the second vertical axis. Similarly, as in the first simulation system, at the initial time t = 0 the system is equipped with the buffer vessel at its maximum capacity. Hence, according to the simulation, in the initial intervals, the system does not need to operate and the set point *SP* is equal to 0. Only when the buffer vessel capacity drops below its minimum, due to occurred heat demand and the little influence of the heat losses (not including convection losses), the system starts operating. In Figure 34 one can see that the system operates more frequently when there is a higher heat power required. In each iteration, the electrical energy produced is calculated and the fuel energy consumption and then summed up. As a result, the overall cost is evaluated.

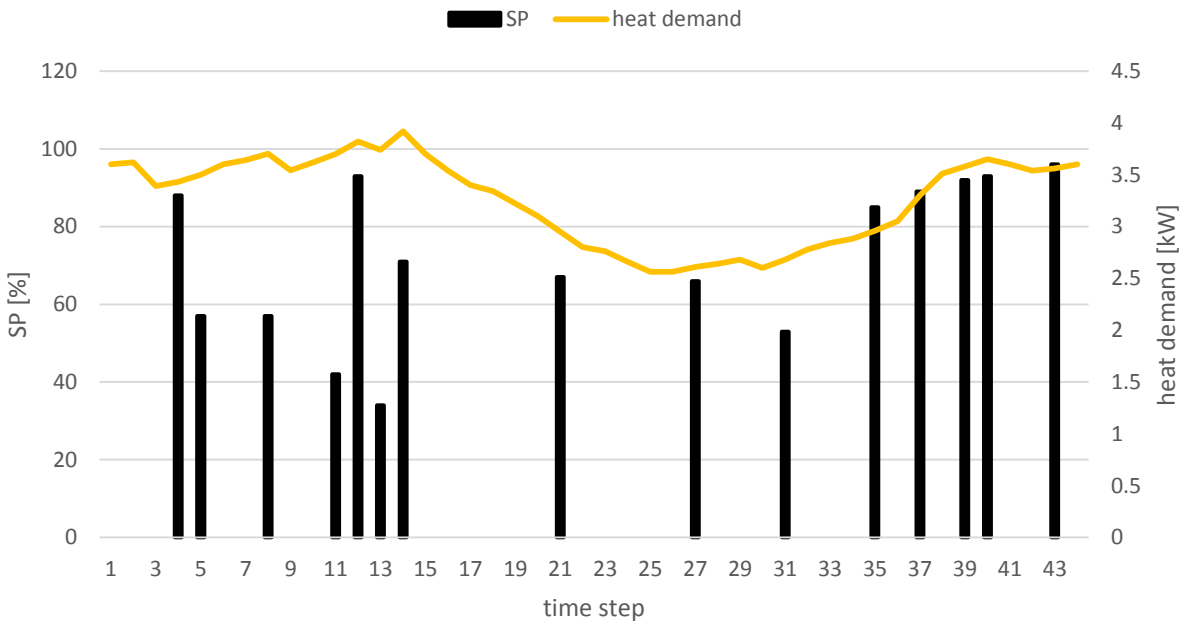

Figure 34 Simulated operating schedule of the system operations in part load with restriction to the total heat demand

Table 7 presents the results of the simulations of the numerical model for two cases (part load and full load operation) with restriction to the demand of heat for sanitary hot water and space heating. The first column of the Table 7 shows the output of the objective function of the optimization model, which is the final minimized cost. The final minimized cost is the overall economic cost of the electrical energy produced and the fuel energy consumed during the system operation for a 24 h simulation time. The positive value of the final minimized cost means that the economic value of the total consumed energy is greater than the economic value of the total produced electrical energy (see Equation (25)). Since the fuel consumed due to the system operation is the cost for the user, it is desirable to have a value as low as possible for the lower positive value of the final minimized cost. If the final minimized cost was negative, it would mean the

user would earn money with the corresponding system operation mode. This can happen because the user does not have to buy electricity at state prices and can obtain the subsidies for the production of electricity. The next two columns in **Error! Not a valid bookmark self-reference.** represent the total produced electric energy and the total consumed fuel energy for a 24h-simulation time. As a result, it can be concluded that this simulation operation in full load has led to the lower economic costs than the operation in part load.

Table 7 Comparison of the simulation results of the numerical model in part load and full load operation with restriction to the total heat demand profile

	final minimized cost [EUR]	**total produced electric energy [kWh]**	**total consumed fuel energy [kWh]**
full load	2.41	17.77	122.03
part load	3.03	17.13	128.70

5.2. Results only for SHW

5.2.1. Operation at full load

Figure 35 represents results of the numerical model simulation of the system operation in full load with respect to the heat demand for sanitary hot water (orange line). The SHW profile is characterized by a few zero heat power demand values (i.e. due to no need for hot water from customers during the night). This results in a different operational schedule of the system than for the heat profile with the constant demand of heat. Only, at the 12^{th} time interval, so after 22 000 s (more than 6 hours) should the system start operating according to the simulation. After that time, the buffer vessel capacity reached its minimum due to the consumption of heat from BV and heat losses. For the total considered simulation time (24 h), nine starts of the system occur, corresponding to the black bars on Figure 35. The number of starts in this simulation is lower than for the simulation from the section above, where the heat demand was greater than zero for each iteration time and the power values of demanded heat were different.

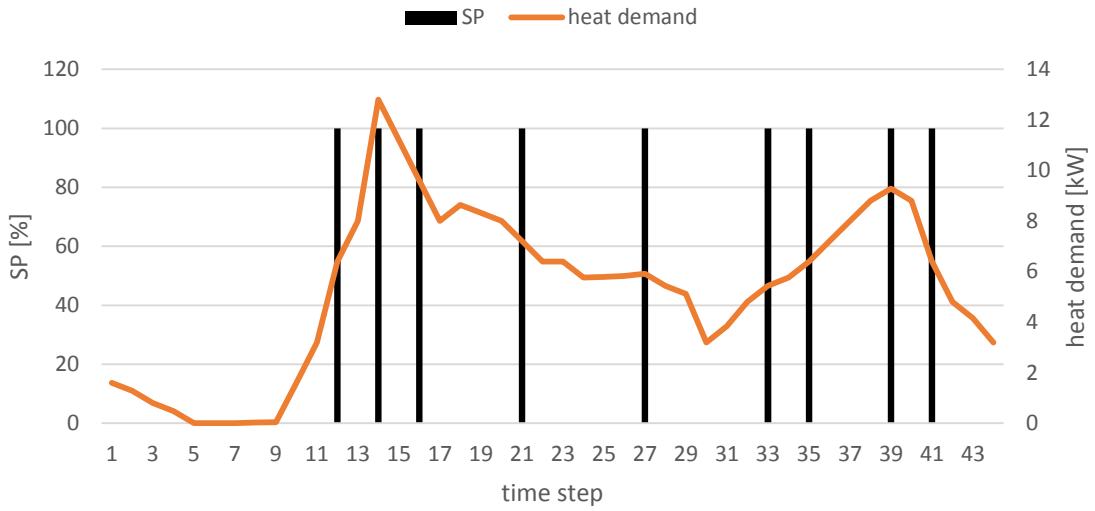

Figure 35 Simulated operating schedule of the system operations in full load with restriction to the SHW heat demand

5.2.2. Operation at part load

Figure 36 represents the simulation results of the numerical model of the system operation in part load with respect to heat for sanitary hot water (orange line). As expected, similarly to the simulation of full load operation with the same heat demand, from Figure 36, it can be seen that the system should start operating only after 11 steps of iteration. The number of starts of the system according to this simulation should be 11 to comply with the heat demand and it is greater than for the operation at full load.

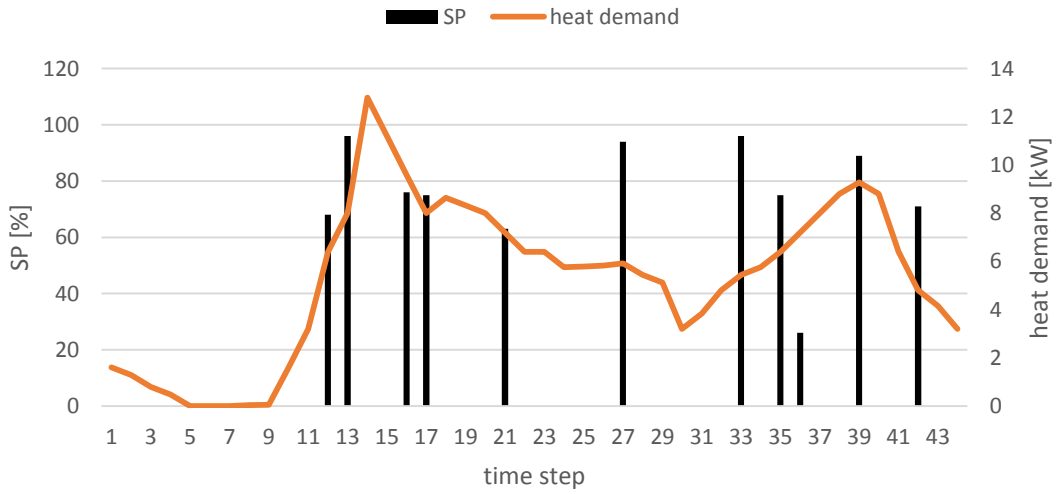

Figure 36 Simulated operating schedule of the system operations in part load with restriction to the SHW heat demand

Table 8 represents the comparison of the simulation results of the numerical model of the system operating in full load and in part load with respect to the demand of heat for sanitary hot water. Similarly to Table 7, the first column of represents values of the minimized cost of operating the system in full load and part load. The second and the third columns show the total produced electric energy and consumed fuel energy during the operation scheme presented on Figure 35 and Figure 36, respectively. As in the case of the simulation results from section above, operation in full load is more economically efficient to comply with the defined heat demand. However, the difference in values of the final minimized cost is not significant. The benefit of operation in full load, in this case, is smaller than for the case described in the previous paragraph because, according to the simulation results, the difference in the number of the system starts is smaller in this case.

Table 8 Comparison of the simulation results of the numerical model in part load and full load operation

	final minimized cost [EUR]	**total produced electric energy [kWh]**	**total consumed fuel energy [kWh]**
full load	2.06	18.00	117.64
part load	2.49	12.58	98.73

6. Conclusions

6.1. Experimental part

The results of the experiments of the system allow for predicting powers output of the system in various conditions, namely, different loads and different initial temperatures. These parameters are crucial for the system performance since they influence the system efficiencies. Fitting functions to the measurement data can provide values of the produced thermal energy and electricity and consumed fuel during the system operation with a high accuracy (relative error to the measured value is less than 5% for each fitted function).

6.2. The numerical model

Along with this work, the numerical model of the system operation was developed in Python. The result of the numerical model is the objective function that translates the meaning of the economical overall costs of the system operation (micro-CHP and buffer vessel) to comply with two different heat demand profiles. The conclusions from the simulations of the numerical model proved that it is more efficient to operate the system at full load than T part load when the plant is equipped with a buffer vessel of 800 liters and has to comply with the presented heat demand profiles. It means that it is more efficient to start and stop the system more often than to operate it at part load. During start and stop, the system produces electricity and heat production less efficiently than in nominal load. The part load operation is as well characterized by smaller efficiency. Operating at full load with the buffer vessel temperature control results in more intermittent operation of the system and causes efficiency losses. However, according to the work presented in this Thesis, daily operational cost of the micro-CHP is still smaller at full load.

It is essential to operate micro-CHP in an optimal manner in order to decrease the variable costs. When running micro-CHP efficiently, less energy is consumed and therefore, less fuel, which contributes to less emission production. The environmental aspects are one of the drivers encouraging the development of micro-CHP in the market. Due to EU stricter regulations, governments have to find a way to produce energy more efficiently. In terms of economic aspects, micro-CHP fed with the natural gas is especially attractive when having the prices of NG almost five times lower than electricity prices (like in Germany in 2016).

.

6.3. Future work

The presented work can be elaborated in different directions. System modeling was done based on the experimental data. This means that for any other version of the EnerTwin, the model may not be valid. The presented model in all its characteristics (see chapter 3) fit very well in the real performance of the unit but it would be interesting to have a universal model that is based more on physical relations. Usually, this is performed with specific, not open source, software like the one mentioned in the ‘Literature review’ section.

Regarding the numerical model, higher accuracy could be obtained with a shorter time interval (ideally - every second). Another promising direction is to study the performance of the system with different buffer vessel capacities and various economic parameters, namely, electricity prices, subsidies for the electricity production in micro-CHP and natural gas prices. It is worth to recommend the current work for the studying of the operation of micro-CHP units with thermal storage on longer than daily basis (e.g. 1 year). Additionally, the future work may include modifications for various heat demand profiles, different seasons of the year, different building types and geographic regions.

References

1. Houwing M., Ajah A. N., Heijnen P. W., Bouwmans I., Herder P. M. Uncertainties in the design and operation of distributed energy resources: The case of micro-CHP systems. Energy. 2008;33(10):p.1518–1536.

2. Nascimento M. A. R., Rodrigues L., Santos E. C., Gomes E. B., Dias F. L. G., Velásques E.I.G., Carrillo R. A. M. Benini D. E., editor. Progress in Gas Turbine Performance. InTech; chapter 5; ISBN 978-953-51-1166-5. 2013. p.109

3. Chicco G., Mancarella P. Distributed multi-generation: A comprehensive view. Vol. 13, Renewable and Sustainable Energy Reviews. 2009. p. 535–551.

4. Chicco G., Mancarella P. From cogeneration to trigeneration: Profitable alternatives in a competitive market. IEEE Trans Energy Convers. 2006;21(1):p.265–272.

5. Cogen Europe (Cogen). Micro-CHP fact sheet United Kingdom. 2005.

6. CODE2 - Cogeneration Observatory and Dissemination Europe. European cogeneration roadmap. 2015;(January).

7. Darrow K., Tidball R., Wang J., Hampson A. Catalog of CHP Technologies. 2017. Available from: http://www.epa.gov/chp/documents/catalog_chptech_full.pdf ; p.1-6; [cited 2017-09-08]

8. Pellegrino S, Lanzini A, Leone P. Techno-economic and policy requirements for the market-entry of the fuel cell micro-CHP system in the residential sector. Appl Energy. 2015;143:p.370–382.

9. Minciuc E., Le Corre O., Athanasovici V., Tazerout M., Bitir I.. Thermodynamic analysis of tri-generation with absorption chilling machine. Vol. 23, Applied Thermal Engineering. 2003. p. 1391–1405.

10. Elhadidy M. A. Performance evaluation of hybrid (wind/solar/diesel) power systems. Renewable Energy. 2002;26(3):p.401–413.

11. Caliano M., Bianco N., Graditi G., Mongibello L.. Economic optimization of a residential micro-CHP system considering different operation strategies. Appl Therm Eng. 2016;101:p.592–600.

12. Magnani S., Pezzola L., Danti P. Design optimization of a heat thermal storage coupled with a micro-CHP for a residential case study. ScienceDirect. Energy Procedia. 2016;101:p.830–837.

13. Ondeck A., Edgar T. F., Baldea M. A multi-scale framework for simultaneous optimization of the design and operating strategy of residential CHP systems. Appl Energy. 2017;205:p.1499–1511.

14. Camporeale S. M., Fortunato B., Torresi M., Turi F., Pantaleo A.M., Pellerano A. Part Load Performance and Operating Strategies of a Natural Gas—Biomass Dual Fueled Microturbine for

Combined Heat and Power Generation. J Eng Gas Turbines Power. 2015;137(12):p.121-401. Available from: http://gasturbinespower.asmedigitalcollection.asme.org/article.aspx?doi=10.1115/1.4030499

15. Visser W. P. J., Shakariyants S., Later M. T. L., Ayed A. H., Kusterer K. PERFORMANCE OPTIMIZATION OF A 3KW MICROTURBINE FOR CHP APPLICATIONS. ASME. 2012;p.1–10.

16. Homemicro.co.uk. Thermal Storage Vessel Sizing. LZC Technol HVAC, Comput CAD too! 2016;p.1–18.

17. MTT. Installation Manual. Eindhoven; 2017.

18. Baker J. New technology and possible advances in energy storage. Energy Policy. 2008;36(12):p.4368–4373.

19. Dincer I., Rosen M. A. Exergy Analysis of Heating, Refrigerating and Air Conditioning: Methods and Applications. 2015. Elsevier; chapter 1. ISBN: 978-0-12-417203-6. p.10-12.

20. Schütz T., Harb H., Streblow R., Müller D. Comparison of models for thermal energy storage units and heat pumps in mixed integer linear programming. 28th International Conference on Efficiency, Cost, Optimization, Simulation and Environmental Impact of Energy Systems (ECOS), At Pau, FranceAachen. 2015

21. Collazos A, Maréchall F., Gähler C. Predictive optimal management method for the control of polygeneration systems. Comput Chem Eng. 2009;33(10):p.1584–1592.

22. NETZSCH-Gerätebau GmbH. Thermal Insulation Materials Material Characterization, Phase Changes, Thermal Conductivity [Internet]. [cited 2017.09.11]. Available from: https://dcyd0ggl1hia3.cloudfront.net/media/thermal-analysis/brochures/Thermal_Insulation_Materials_E_0214.pdf?1426281752&Policy=eyJTdGF0ZW1lbnQiOlt7IlJlc291cmNlIjoiaHR0cHM6XC9cL2RjeWQwZ2dsMWhpYTMuY2xvdWRmcm9udC5uZXRcL21lZGlhXC90aGVybWFsLWFuYWx5c2lzXC9icm9

23. Natural gas price statistics - Statistics Explained. 2017 [cited 2017.10.10]. Available from: http://ec.europa.eu/eurostat/statistics-explained/index.php/Natural_gas_price_statistics

24. Electricity price statistics - Statistics Explained. 2017 [cited 201710.10]. Available from: http://ec.europa.eu/eurostat/statistics-explained/index.php/Electricity_price_statistics

25. Gailfuß M. New CHP Act in Germany has moderate expansion target. 2016 [cited 2017.09.30]. Available from: http://www.kwkg2016.de/en/current-issues-chp-act-2016/new-chp-act-in-germany-has-moderate-expansion-target.html

26. Fischer D, Wolf T, Scherer J, Wille-Haussmann B. A stochastic bottom-up model for space heating

and domestic hot water load profiles for German households. Energy Build. 2016;124:p.120–128.

27. Antoniou A., Lu W. S. Practical optimization: Algorithms and engineering applications. Practical Optimization: Algorithms and Engineering Applications. Springer; chapter1. ISBN-10: 0-387-71106-6. 2007. p.3-4.

Appendix A

Python optimization algorithm

```
from __future__ import division, print_function
from functools import partial

import numpy as np
from scipy.optimize import minimize
import scipy.optimize
import math
import itertools
import optunity
from sys_fun import *
from load import load

# constant values of electricity, heat and time to stop the sytem (until N1 = 0), unit = kWh and time in sec, N1 being a speed of the turbine
Eel_stopping = 0.010937165
Eth_stopping = 0.45448451
tstopping = 150
p_el_buy =0.006
p_el_sub = 0.298
p_f = 0.064
tstarting = 2000
cp = 4.19 / 3600  # water specific heat in kWh/(kg*K)
# find the minimum buffer vessel (BV) surface area having as input data volume and constraint that radius has to be higher than 0.15m
# initial_dimenstions[0] = r; initial_dimenstions[1] = H
initial_dimenstions = [1, 1]

def BV_surfacearea(initial_dimenstions):
    A = 2 * math.pi * initial_dimenstions[0] * (initial_dimenstions[0] + initial_dimenstions[1])
    return A
V_init = 800 / 1000
def BV_volume(initial_dimenstions):
    V = math.pi * initial_dimenstions[0] ** 2 * initial_dimenstions[1]
    return V

def BV_volume_eq(initial_dimenstions, V_init=1):
    return BV_volume(initial_dimenstions) - V_init

cons = {'type': 'eq', 'fun': partial(BV_volume_eq, V_init=V_init)}
res = minimize(BV_surfacearea, initial_dimenstions, method='SLSQP',
               bounds=[(0.15, 1000), (0.15, 100)],
               constraints=cons, options={'disp': False})
# print(res)
A = BV_surfacearea(res.x)  # calculate sufrace area with the solution from minimalization
h = 0.3  # heat coeff W/m2K used to calculate heat losses to the environment
Tenv = 293  # environment temperature [K]
T0 = 293.15  # inital BV temperature [K]
TB_max = 353.15  # maximum BV temperature[K]
TB_min = 333.15  # temperature to start the system, trigger point [K]

V = BV_volume(res.x)
Bmax = 1000 * V * (TB_max - T0) * cp  # max BV capacity [kWh]
print('Bmax', Bmax)
Bmin = 1000 * (TB_max - TB_min) * cp * V  # decrease in BV capacity that will trigger starting the system [kWh]
print('Bmin', Bmin)

time_interval = 2000
```

```
time_total = 24 * 60 * 60
time_steps = tuple(np.arange(0, time_total, time_interval))

assert len(load) == len(time_steps)
B0 = Bmax  # (Bmax - Bmin) / 2  # initial buffer vessel capcity
T0 = TB_max
n_eval = int(100000)
bounds = [(-20, 100)] * len(time_steps)
binary = True

class memoize(dict):
    def __init__(self, func):
        self.func = func

    def __call__(self, *args, **kwargs):
        if args not in self:
            self[args] = self.func(*args, **kwargs)
        return self[args]

@memoize
def cost_and_b(pc_control, time_steps, Bstart, Tstart, load, verbose=False):
    cost_total = 0  # total cost
    total_Eth = 0
    total_Eel = 0
    total_Ef = 0
    #costmoney_total = 0
    t_stop = 0  # time of the last system stop
    bs = np.zeros(len(time_steps))  # BV capacity at timesteps
    for i_t in range(len(time_steps)):

        t1 = time_steps[i_t]
        if i_t == len(time_steps) - 1:
            t2 = time_total
        else:
            t2 = time_steps[i_t + 1]

        if pc_control[i_t] < 20:  # now is off
            if i_t > 0 and pc_control[i_t - 1] < 20:  # still off
                the_Eth = Eth_cooling(t1, t2, t_stop)
                the_Eel = Eel_cooling(t1, t2, t_stop)
                the_Ef = 0
            elif i_t > 0:  # was on now off
                assert t2 - t1 > tstopping
                t_stop = t1 + tstopping
                the_Eth = Eth_stopping + Eth_cooling(t1 + tstopping, t2, t_stop)
                the_Eel = Eel_stopping + Eel_cooling(t1 + tstopping, t2, t_stop)
                the_Ef = 0
            else:  # first period and still off
                the_Eth = Eth_cooling(t1, t2, t_stop)
                the_Eel = Eel_cooling(t1, t2, t_stop)
                the_Ef = 0
        else:  # now is on
            # assert t2 - t1 > tstarting
            if i_t > 0 and pc_control[i_t - 1] < 20:  # was off now on
                the_Eth = Eth(t1 - t_stop,
                              pc_control[i_t])  # + Eth_stst(t2 - t1 - tstarting, pc_control[i_t])
                the_Eel = Eel(t1 - t_stop,
                              pc_control[i_t])  # + Eel_stst(t2 - t1 - tstarting, pc_control[i_t])
                the_Ef = Ef(t1 - t_stop,
                            pc_control[i_t])  # + Ef_stst(t2 - t1 - tstarting, pc_control[i_t])
                if t2 - t1 > tstarting:
                    the_Eth += Eth_stst(t2 - t1 - tstarting, pc_control[i_t])
```

```
                the_Eel += Eel_stst(t2 - t1 - tstarting, pc_control[i_t])
                the_Ef += Ef_stst(t2 - t1 - tstarting, pc_control[i_t])

            elif i_t > 0:  # still on
                the_Eth = Eth_stst(t2 - t1, pc_control[i_t])
                the_Eel = Eel_stst(t2 - t1, pc_control[i_t])
                the_Ef = Ef_stst(t2 - t1, pc_control[i_t])
            else:  # first period
                the_Eth = Eth(t1 - t_stop, pc_control[i_t])  # + Eth_stst(t2 - t1 - tstarting,
                # pc_control[i_t])
                the_Eel = Eel(t1 - t_stop, pc_control[i_t])  # + Eel_stst(t2 - t1 - tstarting,
                # pc_control[i_t])
                the_Ef = Ef(t1 - t_stop, pc_control[i_t])  # + Ef_stst(t2 - t1 - tstarting,
                # pc_control[i_t])
                if t2 - t1 > tstarting:
                    the_Eth += Eth_stst(t2 - t1 - tstarting, pc_control[i_t])
                    the_Eel += Eel_stst(t2 - t1 - tstarting, pc_control[i_t])
                    the_Ef += Ef_stst(t2 - t1 - tstarting, pc_control[i_t])
        if verbose:
            print('time=%d, Eth: %.3f, Eel: %.3f, Ef: %.3f, BV=%.3f PC=%d' % (t2,the_Eth,the_Eel,the_Ef, Bstart
pc_control[i_t]))

        Bstart = Bstart + the_Eth - load[i_t]
        Tend = Bstart / (cp * V * 1000) + T0
        Benv = h / 1000 * A * ((Tend + Tstart) / 2 - Tenv) * ((t2 - t1) / 3600)
        Bstart -= Benv
        Tstart = Tend
        Bstart = max(Bstart, 0)

        cost_i = -1 * the_Eel * (p_el_buy + p_el_sub) + 1 * the_Ef * p_f
        #costmoney_i = -1 * the_Eel * 0.302 + 1 * the_Ef * 0.064
        bs[i_t] = Bstart
        cost_total += cost_i
        total_Eth += the_Eth
        total_Eel += the_Eel
        total_Ef += the_Ef

        #costmoney_total += costmoney_i
    print('total Eth=', total_Eth)
    print('total Eel=', total_Eel)
    print('total Ef=', total_Ef)

    return cost_total, bs, total_Eth

def cost_only(pc_control, time_steps, Bstart, Tstart, load, verbose=False):
    return cost_and_b(pc_control, time_steps, Bstart, Tstart, load, verbose=verbose)[0]

def b_only(pc_control, time_steps, Bstart, Tstart, load):
    return cost_and_b(pc_control, time_steps, Bstart, Tstart, load)[1]

cost = partial(cost_only, time_steps=time_steps, Bstart=B0, Tstart=T0, load=load)
b = partial(b_only, time_steps=time_steps, Bstart=B0, Tstart=T0, load=load)

def whole_x_constraint(**kwargs):
    pc = x_from_kwargs(kwargs)
    bs = b(pc)
    bs = [B0] + list(bs)
    for i in range(0, len(time_steps)):
        if bs[i] >= Bmax and pc[i] >= 20:
            return False  # r[i - 1] - Bmax
        if bs[i] <= Bmax - Bmin and pc[i] < 20:
            return False  # Bmin - r[i - 1]
```

```
    return True

def x_from_kwargs(kwargs):
    values = list(map(lambda kv: kv[1], sorted(kwargs.items(), key=lambda x: int(x[0][1:3]))))
    # x = np.array(values)
    x = tuple(values)
    return x

def cost_2(**kwargs):
    x = x_from_kwargs(kwargs)
    c = cost(x)
    print(x, c)
    return c

cost_constrained = optunity.wrap_constraints(cost_2, custom=[whole_x_constraint])

import tqdm
tq = tqdm.tqdm(total=n_eval)

def binary_pc(**kwargs):
    kwargs = {k: 100 if v >= 20 else 0 for k, v in kwargs.items()}
    return kwargs

def variable_pc(**kwargs):
    kwargs = {k: int(v) if v >= 20 else 0 for k, v in kwargs.items()}
    return kwargs

if binary:
    x_transform = binary_pc
else:
    x_transform = variable_pc

def cost_tqdm(**kwargs):
    tq.update(1)
    return cost_constrained(**x_transform(**kwargs))
res = optunity.minimize(cost_tqdm,solver_name='random search', num_evals=n_eval,
                        **{'x%d' % i: b for i, b in enumerate(bounds)})
print('Optimizer response')
print(res)
x = x_transform(**res[0])
print('Does x satisfy constraints?')
print(whole_x_constraint(**x))
res = x_from_kwargs(x)
print('PC: ')
print(res)
print('Cost: ')
cost_and_b.clear()
print('final minimized cost is=',cost_and_b(res, time_steps, B0, T0, load, True)[0])
for bb, pc in np.vstack([b(res), res]).T:
    print('%.3f\t\t %.3f' % (np.round(pc), np.round(bb, 3)))

exit()
```

Appendix B

Functions in Python

```
# functions describing system performance

import random
# functions for cooling; t-cooling time
def Pel_cooling(t):
    electricity_cooling = -0.00001140346314178 67 * (t) - 0.00894725923427203
    return electricity_cooling

def Eel_cooling(t1, t2, t_stop):
    pt1 = Pel_cooling(t1 - t_stop)
    pt2 = Pel_cooling(t2 - t_stop)
    return pt2 - pt1


def Eth_cooling_before_2350(t):
    heat_cooling = 0.000180876281808513 * (t) + 0.00934463874989772
    return heat_cooling


def Eth_cooling_between_2350_and_9007(t):
    heat_cooling = 0.0000342319746331191 * (t) - 0.0170401903251734
    return heat_cooling


def Eth_cooling_after_9007(t):
    return 0  # Eth_cooling_between_2350_and_9007(6657) + Eth_cooling_before_2350(2350)


def intersect_interval(x, y):
    start = max(x[0], y[0])
    end = min(x[1], y[1])
    return min(start, end), end


def Eth_cooling(t1, t2, t_stop):
    # t_since_stop = t1 - t_stop
    # t_between = t2 - t1
    t_2350 = t_stop + 2350
    t_9007 = t_stop + 9007
    tt_below = (t_stop, t_2350)
    tt_between = (t_2350, t_9007)
    tt_after = (t_9007, t2)
    my_interval = (t1, t2)

    time_before = intersect_interval(my_interval, tt_below)
    time_between = intersect_interval(my_interval, tt_between)
    time_after = intersect_interval(my_interval, tt_after)
    return Eth_cooling_before_2350(time_before[1]) - Eth_cooling_before_2350(time_before[0]) + \
        Eth_cooling_between_2350_and_9007(time_between[1]) -
Eth_cooling_between_2350_and_9007(time_between[0]) + \
        Eth_cooling_after_9007(time_after[1]) - Eth_cooling_after_9007(time_after[0])

# below is calculation of Tt34_0 - starting temperature of the system for the 2nd time. Tt34_0 depends on cooling
time
def Tt34_0(tcooling):
```

```
    temp_Tt34_0 = (-0.000000000000000000000101796228 * (tcooling) ** 5 + 0.0000000000000000257877045721949
* (tcooling) ** 4 - 0.000000000025382273947983 5 * (tcooling) ** 3 + 0.00000125616668557971 * (tcooling) ** 2 -
0.0352379324593812 * (tcooling) + 886.183648200713)
    return temp_Tt34_0

# below there are functions calculating fuel energy, electric and thermal energy depending on two variables: Tt_34_0
and PC
# Tt34_0 on the other hand depends on cooling time before start and is described with the other function.
# so at the end energies for start will depend on cooling time and PC
# fuel energy for the start depending on the Tt34_0

def Eth(tcooling, PC):
    return -3.4047844698339644e-06 * Tt34_0(tcooling) ** 2. + 0.0004538840898995127 * PC ** 2. + \
        3.422097022388708e-06 * Tt34_0(tcooling) * PC + 0.007038543785845651 * Tt34_0(tcooling) - \
        0.005975737879632128 * PC + 1.2581319432016065

def Eel(tcooling, PC):
    return -1.027672065274975e-06 * Tt34_0(tcooling) ** 2. + 9.353834691480387e-05 * PC ** 2. + \
        6.644049794636553e-06 * Tt34_0(tcooling) * PC + 0.0011588837101124529 * Tt34_0(tcooling) - \
        0.0017349487390934315 * PC + 0.08778375668595234

def Ef(tcooling, PC):
    return 8.502902169261681e-07 * Tt34_0(tcooling) ** 2. + 0.0005198290988392521 * PC ** 2. + \
        4.765668172663438e-05 * Tt34_0(tcooling) * PC - 0.005767325835948347 * Tt34_0(tcooling) - \
        0.03894860976388058 * PC + 9.99124062223132

# energy in steady state as a function of the load (PC) and time
def Fuel_power_stst(PC):
    fuel_power = 0.00141192392482067000 * PC ** 2 - 0.03166862022438700000 * PC + 9.54222819481281000000
    return fuel_power

def Ef_stst(t, PC):
    fuel_energy = Fuel_power_stst(PC) * t / 3600
    return fuel_energy

def Electric_power_stst(PC):
    electric_power = 0.00025113112913590500 * PC ** 2 - 0.00011597628916976100 * PC +
0.78869434426078300000
    return electric_power

def Eel_stst(t, PC):
    electric_energy = Electric_power_stst(PC) * t / 3600
    return electric_energy

def Thermal_power_stst(PC):
    thermal_power = 0.00104983333333335000 * PC ** 2 - 0.01850500000000190000 * PC +
7.55216666666675000000
    return thermal_power

def Eth_stst(t, PC):
    thermal_energy = Thermal_power_stst(PC) * t / 3600
    return thermal_energy
```